MCM10 compensates for Myc-induced DNA replication stress in breast cancer stem-like cells

Takahiko Murayama[1,2], Yasuto Takeuchi[2], Kaoru Yamawaki[3,4], Toyoaki Natsume[5,13], Rojas-Chaverra N. Marcela[2], Tatsunori Nishimura[2], Yuta Kogure[6], Asuka Nakata[2,7], Kana Tominaga[1,2,3], Asako Sasahara[1,8], Masao Yano[9], Satoko Ishikawa[10], Tetsuo Ohta[10], Kazuhiro Ikeda[11], Kuniko Horie-Inoue[11], Satoshi Inoue[11], Masahide Seki[12], Yutaka Suzuki[12], Sumio Sugano[12], Takayuki Enomoto[4], Masahiko Tanabe[8], Kei-ichiro Tada[8], Masato T. Kanemaki[5,13], Koji Okamoto[3], Arinobu Tojo[1], Noriko Gotoh[1,2*]

[1]Division of Molecular Therapy, Institute of Medical Science, The University of Tokyo, Minato-ku, Tokyo, Japan

[2]Division of Cancer Cell Biology, Cancer Research Institute, Kanazawa University, Kanazawa City, Ishikawa, Japan

[3]Division of Cancer Differentiation, National Cancer Center Research Institute, Chuo-ku, Tokyo, Japan

[4]Department of Obstetrics and Gynecology, Graduate School of Medical and Dental Sciences, Niigata University, Niigata, Japan

[5]Department of Chromosome Science, National Institute of Genetics, Research Organization of Information and Systems (ROIS), Mishima City, Shizuoka, Japan

[6]Department of Computational Biology and Medical Sciences, Graduate School of Frontier Science, The University of Tokyo, Kashiwa City, Chiba, Japan

[7]Department of Pediatrics, Faculdade de Medicina, Universidade de São Paulo, São Paulo, Brazil

[8]Department of Breast & Endocrine Surgery, Graduate School of Medicine, The University of Tokyo, Bunkyo-ku, Tokyo, Japan

[9]Department of Surgery, Minamimachida Hospital, Machida City, Tokyo, Japan

[10]Department of Gastroenterological Surgery, Kanazawa University, Kanazawa City, Ishikawa, Japan

[11]Division of Gene Regulation and Signal Transduction, Research Center for Genomic Medicine, Saitama Medical University, Hidaka City, Saitama, Japan

[12]Department of Medical Genome Sciences, Graduate School of Frontier Sciences, The University of Tokyo, Kashiwa City, Chiba, Japan

[13]Department of Genetics, SOKENDAI, Mishima City, Shizuoka, Japan

Running title: MCM10 maintains CSCs in c-Myc-induced DNA replication stress

Corresponding Author:

Noriko Gotoh, MD, PhD

Email: ngotoh@staff.kanazawa-u.ac.jp

Phone: +81 762646730

Kakuma-machi, Kanazawa City, Ishikawa 920-1192, Japan

Disclosure of Potential Conflicts of Interest;

The authors declare no potential conflicts of interest.

Abstract

Cancer stem-like cells (CSCs) are responsible for the drug resistance of tumors and recurrence while they experience DNA replication stress. However, the underlying mechanisms that cause DNA replication stress in CSCs and how they compensate for this stress remain unclear. Here we provide evidence that upregulated c-Myc expression induces stronger DNA replication stress in patient-derived breast CSCs than in differentiated cancer cells. Our results suggest critical roles for mini-chromosome maintenance protein 10 (MCM10), which is a firing (activating) factor of the DNA replication origins, to compensate for the DNA replication stress. Expression levels of MCM10 are upregulated in CSCs and maintained by c-Myc. c-Myc-dependent collisions may take place between RNA transcription and DNA replication machinery in nuclei, thereby causing DNA replication stress. MCM10 may activate dormant replication origins close to the collisions to ensure replication progression. Moreover, patient-derived breast CSCs were dependent on MCM10 for their maintenance even after enrichment for CSCs that were resistant to paclitaxel, the standard chemotherapeutic agent. In addition, MCM10 depletion decreased the growth of cancer cells but not normal cells. Therefore, MCM10 is likely to robustly compensate for DNA replication stress and facilitate genome duplication in the S-phase in cancer cells, which is more pronounced in CSCs. We provide a preclinical rationale to target the c-Myc-MCM10 axis to prevent drug resistance and recurrence.

Introduction

Breast cancer is the most frequently observed tumor type among women worldwide. Some breast cancer patients show poor prognosis due to resistance to therapy and tumor recurrence (Torre et al., 2015). Over the past few decades, studies have shown that a subset of cancer cells have the capacity to initiate tumors (Batlle & Clevers, 2017; Saygin, Matei, Majeti, Reizes, & Lathia, 2019). These tumor-initiating cells or cancer stem-like cells (CSCs) are resistant to conventional chemotherapeutic agents, resulting in recurrence. To improve the prognosis of breast cancer patients, CSC-targeted therapeutic strategies are urgently required. Clarification of the features of CSCs is important to develop CSC-targeting therapy to remove the cells and prevent recurrence. *In vitro* tumor spheroid formation in serum-free floating culture conditions was established to enrich CSCs (Ablett, Singh, & Clarke, 2012; Ponti et al., 2005) . Researchers, including our group, have used this method to shed light on the features of CSCs (Beier et al., 2007; Clement, Sanchez, de Tribolet, Radovanovic, & Ruiz i Altaba, 2007; Hinohara et al., 2012; Murayama et al., 2016; Sansone et al., 2007; Tominaga et al., 2019). Although the features of CSCs have been studied extensively, the roles of DNA replication initiation factors in CSCs have not been studied carefully.

In preparation for cell division, the whole genome must be replicated during the S-phase of the cell cycle. To rapidly generate a complete copy of the entire genome, replication of the eukaryotic genome is initiated from thousands of origins (Fragkos, Ganier, Coulombe, & Mechali, 2015; Masai, Matsumoto, You, Yoshizawa-Sugata, & Oda, 2010). The inactive MCM2–7 helicases (composed of MCM family proteins MCM2, MCM3, MCM4, MCM5, MCM6, and MCM7) bind to numerous sites of origins of DNA replication on the genome to form pre-replicative complexes (pre-RCs) in late M- and G1-phases. Following the activation of S-phase cyclin-dependent kinase (S-CDK) in the S-phase, MCM2-7 in pre-RCs are activated to form the CDC45/MCM2-7/GINS (CMG) helicase, and only ~1/10 of the chromatin-bound MCM2-7 are converted into the CMG helicase in normal cells. Subsequent recruitment of firing (activating) factors including MCM10 activates the CMG helicase to form the replisome that includes DNA polymerases, followed by

initiation of bidirectional DNA replication (Douglas, Ali, Costa, & Diffley, 2018; Gambus et al., 2006; Kanke, Kodama, Takahashi, Nakagawa, & Masukata, 2012; Looke, Maloney, & Bell, 2017; van Deursen, Sengupta, De Piccoli, Sanchez-Diaz, & Labib, 2012; Watase, Takisawa, & Kanemaki, 2012). MCM10 opens the MCM2–7 ring within CMG, creating a single-stranded DNA gate for passing one DNA strand when the CMG helicase engages in fork progression (Wasserman, Schauer, O'Donnell, & Liu, 2019). On the other hand, most of the origins remain dormant, and those pre-RCs are passively removed from DNA when the replisomes approach the dormant origins during replication progression.

DNA replication stress is defined as the stalling or slowing of replication progression due to interference with the normal replication process by a variety of mechanisms, including DNA strand breaks, lack of nucleotides, etc. (Techer, Koundrioukoff, Nicolas, & Debatisse, 2017; Zeman & Cimprich, 2014). Recently, a repair process that responds to DNA strand breaks has received much attention as a potential therapeutic target. Inhibitors of poly (ADP-ribose) polymerase (PARP), a repair enzyme for single strand breaks, are clinically used in breast cancer patients with *BRCA* mutations (Pettitt & Lord, 2019). However, in the majority of patients without *BRCA* mutations, PARP inhibitors are not clearly effective. In cancer cells, constitutive activation of oncogenes is a primary cause of replication stress (Gaillard, Garcia-Muse, & Aguilera, 2015; Kotsantis, Petermann, & Boulton, 2018; Petropoulos, Champeris Tsaniras, Taraviras, & Lygerou, 2019). Although it was reported that glioblastoma stem cells suffer from upregulated DNA replication stress (Carruthers et al., 2018), the level of DNA replication stress in other types of CSCs, including breast CSCs, remains unknown. When cells suffer from replication stress, checkpoint pathways are activated (Kotsantis et al., 2018) (Petropoulos et al., 2019) (Blow & Ge, 2009). Ataxia telangiectasia- and Rad 3-related protein (ATR) kinase, and subsequently checkpoint kinase 1 (Chk1), are phosphorylated and activated. Activated Chk1 slows down cell cycle progression in the S-phase and creates a time for the dormant origins to be activated for

116 completion of DNA replication. Many proteins included in the aforementioned DNA replication
117 initiation machinery work together to activate the dormant origins.

118 *c-Myc* is a typical oncogene that is frequently overexpressed in numerous cancer types. The
119 transcription factor c-Myc is able to induce transcription of ~15% of whole genes in the genome
120 (Meyer & Penn, 2008). Although transcription in the G1-phase is sequentially followed by DNA
121 replication in the S-phase in normal cells, c-Myc overexpression disrupts the cooperation between
122 the transcription and replication machinery (Macheret & Halazonetis, 2018). As a result, they
123 collide on the DNA strands, leading to DNA replication stress in cancer cells.

124 To clarify the specific features of CSCs in this study, we examined breast cancer patient-derived
125 primary samples. We compared whole transcriptomes of CSC-enriched spheroid cells and
126 cultured cells in the regular adherent condition. We found that pathways contributing to c-Myc
127 activation and DNA replication stress were upregulated in CSC-enriched spheroid cells. Our
128 results suggest that c-Myc causes frequent collisions between the transcription and replication
129 machinery in the nuclei. Theses collisions may be one of the major causes of higher levels of
130 DNA replication stress in CSCs compared to differentiated cancer cells. Further, we showed that
131 the expression levels of MCM10 were increased in CSCs and differentiated cancer cells, and that
132 expression was higher in the former than the latter, compared to normal cells. MCM10 may
133 compensate for such replication stress by activating the dormant origins. Moreover, we
134 demonstrated that MCM10 plays critical roles in the maintenance of CSCs, even those that are
135 resistant to paclitaxel, a commonly used chemotherapeutic agent for breast cancer. Furthermore,
136 by analyzing patient-derived cancer cells (PDCs), we found that MCM10 is also essential for the
137 growth of differentiated cancer cells. Thus, inhibition of MCM10 may be a novel therapeutic
138 strategy that targets replication initiation in CSCs.

139 This study is the first to demonstrate that increased activity of c-Myc is a major cause of DNA
140 replication stress in breast CSCs. Furthermore, a c-Myc-dependent firing factor, MCM10, which

is required for activation of the replisome, is essential for CSCs, probably for compensating for DNA replication stress.

Results

CSCs can be enriched in the spheroid culture condition and show distinct features

To identify specific features of CSCs, we first cultured patient-derived breast cancer cells both in the spheroid condition, in which cells are cultured in sphere culture medium (SCM) on ultra-low attachment dishes, and in the normal adherent condition (Fig. 1a). Spheroid cells retain their stem cell features, such as high tumor-initiating ability and expression of stemness marker proteins (Ablett et al., 2012; Dontu, Al-Hajj, Abdallah, Clarke, & Wicha, 2003; Murayama et al., 2016). Indeed, patient-derived spheroid cells showed significantly higher tumor-initiating ability *in vivo* compared to their counterparts in the adherent condition (Fig. 1b and Supplementary Fig. 1a). In addition, western blotting revealed that the expression levels of the stemness marker proteins Nanog and Oct-4 were higher in spheroid cells than in adherent cells (Fig. 1c). Immunocytochemistry (ICC) showed that strong Nanog staining was observed in the nucleus and that more spheroid cells were strongly positive for Nanog (Fig. 1d). A subpopulation of breast CSCs is enriched in the $CD24^{low/-}/CD44^{high}$ cell population (Al-Hajj, Wicha, Benito-Hernandez, Morrison, & Clarke, 2003), and thus, we investigated this population with flow cytometry. The proportion of cells in the $CD24^{low/-}/CD44^{high}$ cell fraction was higher in spheroid cells than in adherent cells (Fig. 1e). These results indicate that breast CSCs were more abundant in spheroid cells, whereas differentiated cancer cells were more abundant in adherent cells.

Next, we performed RNA sequencing (RNA-seq) to compare the transcriptomes of spheroid cells and adherent cells (Fig. 1f). All samples were derived from the breast tumor tissues of three individual patients (PDCs #1, #2, and #3; clinical sample information is summarized in Supplementary Table 1). Gene set enrichment analysis (http://software.broadinstitute.org/gsea/index.jsp) based on the RNA-seq data revealed that genes

167 associated with drug resistance and the epithelial-mesenchymal transition were upregulated in
168 spheroid cells compared to adherent cells (Fig. 1g). Because these are well-known features of
169 CSCs, we confirmed that CSCs were enriched in spheroid cells (Zhang & Weinberg, 2018). We
170 also noticed that other gene sets related to Myc targets and the DNA replication stress response
171 were highly upregulated in spheroid cells (Fig. 1g).
172
173 **c-Myc expression is increased in CSC-enriched spheroid cells, which may lead to strong**
174 **DNA replication stress**
175 We then investigated c-Myc protein levels. Western blotting revealed that expression levels of c-
176 Myc were higher in spheroid cells than in adherent cells among all three PDC samples irrespective
177 of the different subtypes (Fig. 1h, triple negative [#1], HER2 [#4], and luminal-like [#6]). ICC
178 showed strong accumulation of c-Myc in the nucleus, and we observed that more spheroid cells
179 were strongly positive for c-Myc than adherent cells (Fig. 1i), suggesting that a subpopulation of
180 CSCs express c-Myc strongly.
181 Because gene sets related to the DNA replication stress response were upregulated in spheroid
182 cells, we next examined the proteins involved in the checkpoint pathways (Kotsantis et al., 2018;
183 Petropoulos et al., 2019). We found that the phosphorylation levels and amounts of ATR and Chk1
184 were higher in spheroid cells than in adherent cells (Fig. 2a). These results suggest that spheroid
185 cells experienced more DNA replication stress that activated the checkpoint pathways. To directly
186 monitor DNA replication fork stalling caused by DNA replication stress, we performed DNA
187 fiber assays (Schwab & Niedzwiedz, 2011). We labeled cells with IdU for 30 min and then with
188 CIdU for the next 30 min (Fig. 2b). Using this approach, bidirectional forks can be observed when
189 a single replication origin is activated in the first 30 min (IdU: green) and then proceeds in two
190 opposite directions (Fig. 2c, left and middle panels). If the two forks proceed normally, a CIdU-
191 labeled (red) fork of the same length should be observed. On the other hand, when one fork stalls
192 because of DNA replication stress, the two forks will have different lengths. We observed fork

193 stalling more frequently in spheroid cells as reflected in the higher frequency of asymmetric
194 CIdU-containing forks (Fig. 2c, right panel). When forks stall during the first 30 min, the stalled
195 forks will be labeled only by IdU (green) (Fig. 2d, left panel). We observed these stalled forks
196 more frequently in spheroid cells (Fig. 2d, right panel). Taken together, we concluded that DNA
197 replication stress is upregulated in CSCs compared to differentiated cancer cells.
198 Upregulation of c-Myc induces collisions between transcription and replication machinery in
199 the nucleus, leading to DNA replication stress (Macheret & Halazonetis, 2018). We hypothesized
200 that upregulated c-Myc in CSCs causes collisions between transcription and replication
201 machinery more frequently than in differentiated cancer cells. The collisions are associated with
202 stabilized R-loops, that is, an RNA/DNA hybrid and the displaced single-stranded DNA behind
203 elongation of RNA polymerases (Gan et al., 2011; Techer et al., 2017). R-loops can be detected
204 with ICC staining with the monoclonal antibody S9.6, which is a widely used tool to recognize
205 RNA/DNA hybrids (Vijayraghavan, Tsai, & Schwacha, 2016). RNA/DNA hybrid foci detected
206 with the S9.6 antibody were localized in the nucleus (Fig. 2e). The staining disappeared following
207 treatment with ribonuclease H (RNaseH), which cleaves RNA strands in the RNA/DNA hybrids,
208 confirming the specificity of the antibody (Fig. 2e). We found that spheroid cells showed a higher
209 number of RNA/DNA foci than adherent cells (Fig. 2f). These results suggest that the collisions
210 between transcription and replication machinery occur more frequently in CSCs than in
211 differentiated cancer cells.
212 We then depleted c-Myc expression by using small interfering RNAs (siRNAs) for *c-Myc* (Fig.
213 3a). The depletion of c-Myc led to a decreased number of RNA/DNA hybrid foci and decreased
214 phosphorylation levels of ATR and ChK1 (Fig. 3b, c). Thus, c-Myc-induced collisions between
215 transcription and replication machinery in the nuclei likely lead to DNA replication stress, which
216 is more frequent in CSCs than in differentiated cancer cells.
217
218 **MCM10 expression is upregulated in CSC-enriched spheroid cells and co-localizes with the**

RNA/DNA hybrid foci in nuclei

Based on the results described above, we expected that CSCs would have mechanisms to manage higher levels of DNA replication stress. We focused our attention on *MCM10*, which was the fifth most highly upregulated gene (Supplementary Table 2), because MCM10 may activate dormant origins to compensate for DNA replication stress (Baxley & Bielinsky, 2017). Western blotting showed that the expression levels of MCM10 were higher in several breast cancer cell lines compared with MCF10A, a normal mammary epithelial cell line (Fig. 4a). We found that the expression level of MCM10 was reduced in *c-Myc*-depleted cancer cells, indicating that MCM10 expression is associated with c-Myc expression (Fig. 4b). qPCR and western blotting showed that expression levels of *MCM10* were higher in spheroid cells compared to adherent cells in several PDCs and breast cancer cell lines (Fig. 4c,d). In addition, expression of *MCM10* was higher in the $CD24^{low/-}/CD44^{high}$ cell population, a subpopulation of CSCs, than in the control population (Supplementary Fig.1b, c).

Further, ICC staining showed that MCM10-positive puncta were present in the nucleus (Fig. 4e). The staining disappeared by depletion of MCM10 by using siRNAs for *MCM10*, confirming the specificity of the antibodies (Fig. 4e and Fig. 5b). The number of MCM10-positive puncta were significantly higher in spheroid cells compared to adherent cells (Fig. 4f). All these results suggest that MCM10 expression is maintained by c-Myc and is upregulated in CSCs.

To test whether MCM10 is recruited close to the collisions between the transcription and replication machinery, we stained PDCs by using the antibodies against MCM10 and S9.6. We found significant co-localization of MCM10-positive puncta and RNA/DNA hybrid foci (Fig. 4g). This result supports the notion that MCM10 is recruited to stalled forks due to the collisions in nuclei. Together, our findings suggest that MCM10 expression is upregulated in both CSCs and differentiated cancer cells, and that expression is higher in the former than the latter, compared to normal cells. Expression of MCM10 may be partly induced by upregulated c-Myc expression. Furthermore, MCM10 may be recruited to stalled forks in nuclei.

MCM10 expression levels are prognostic, and MCM10 plays important roles in proliferation of adherent cells

To examine the clinical relevance of MCM10, we analyzed data obtained from publicly available gene expression profiles of breast cancer tissues (Desmedt et al., 2007; Pawitan et al., 2005). We found that breast cancer patients with high levels of *MCM10* expression had poor prognosis (Fig. 5a), supporting the possibility that MCM10 plays important roles in tumorigenesis. According to the Oncomine database (https://www.oncomine.org), *MCM10* expression was higher in various cancer tissues, including breast and colon cancer, than in their normal counterparts (Supplementary Fig. 2a).

To examine the functions of MCM10 in cancer cells, we depleted MCM10 with siRNAs. We confirmed that two kinds of siRNAs efficiently suppressed expression compared to the control siRNA (siCtrl) (Fig. 5b,c). We evaluated the effect of these siRNAs on proliferation of adherent cells. Knockdown of *MCM10* greatly decreased proliferation of MCF7 (luminal), BT20 (triple negative), and PDC #1 (triple negative) cells relative to a nonspecific control siRNA (siCtrl) (Fig. 5d), indicating that MCM10 is essential for the proliferation of differentiated cancer cells regardless of breast cancer subtype. To verify the requirement of high expression of MCM10 for proliferation in ovarian cancer cells, another type of gynecological cancer cell, we utilized the CRISPR-caspase 9 (Cas9)-mediated conditional knockout system to deplete *MCM10* in patient-derived ovarian cancer cells (PDC#8) (Fig. 5b right panels and c). We found that doxycycline (Dox)-induced depletion of *MCM10* led to a great reduction in cell proliferation of the ovarian cancer cells (Fig.5d). In contrast, knockdown of MCM10 in normal MCF10A cells did not significantly alter proliferation (Supplementary Fig.2b,c). These results suggest that MCM10 plays important roles in the proliferation of differentiated cancer cells but not normal cells.

We next measured DNA replication activity by examining BrdU incorporation. When *MCM10* was depleted in adherent cells, BrdU incorporation was decreased, indicating that DNA

271 replication activity was significantly decreased in *MCM10*-depleted cells (Fig. 5e). Together,
272 these results are consistent with the notion that MCM10 depletion increases DNA replication
273 stress, slows down S-phase progression, and decreases cell proliferation. It appears that MCM10
274 is a limiting factor for dealing with DNA replication stress to complete S-phase, leading to cell
275 proliferation.

276 We next examined whether MCM5, a component in pre-RCs, is a limiting factor for
277 proliferation of cancer cells, to the same extent as MCM10. We depleted MCM5 in MCF7 cells
278 with siRNAs. However, we found that cell proliferation was not significantly altered
279 (Supplementary Fig.3a,b). This result indicates that MCM5 is not a limiting factor for
280 proliferation of cancer cells in this condition. Consistently, a previous report showing that
281 MCM2–7 is highly abundant and that MCM5-depleted cells do not show a significant growth
282 defect in normal culture conditions (Ge, Jackson, & Blow, 2007). We then asked whether MCM10
283 overexpression contributes to dealing with the replication stress and thus promotes cell
284 proliferation. To test this, we first overexpressed MCM10 and found that cell proliferation was
285 not significantly altered by MCM10 overexpression alone (Supplementary Fig. 5c,d). We further
286 treated cells with hydroxyurea (HU), an inhibitor of ribonucleotide reductase, to induce
287 replication stress. Treatment with HU leads to a shortage of the deoxyribonucleotides that are
288 used for DNA synthesis in the S-phase (Vesela, Chroma, Turi, & Mistrik, 2017). As expected,
289 treatment with HU decreased cell proliferation, because cells experienced stronger replication
290 stress (Supplementary Fig. 5e). We found that the decreased cell proliferation was partly restored
291 by MCM10 overexpression when cells were treated with 500 μM HU. In this condition, we found
292 that depletion of MCM5 blocked the restored effects on cell proliferation by MCM10
293 overexpression (Supplementary Fig. 5f). These results suggest that MCM10 overexpression deals
294 with the HU-induced strong replication stress in cooperation with MCM5.

295

296 **MCM10 plays important roles in CSC properties**

297 Next, we focused on the association between MCM10 upregulation and CSCs. To this end, we
298 first examined the effects on tumor sphere-forming capacity. *MCM10* depletion greatly decreased
299 the sphere-forming ability of all tested cancer cells (Fig. 6a). We subsequently examined the
300 proportion of $CD24^{low/-}/CD44^{high}$ cells, a subpopulation of the breast CSCs. The proportion of
301 $CD24^{low/-}/CD44^{high}$ cells was lower in *MCM10*-depleted cells than in control cells (Fig. 6b).
302 Furthermore, the expression levels of Nanog and Oct-4 were lower in *MCM10*-depleted cells than
303 in control cells (Fig. 6c). These results suggest that MCM10 plays an important role in the
304 maintenance of CSCs.

305 We next constructed short hairpin RNAs (shRNAs) against *MCM10* (shMCM10 #1 and #2)
306 and confirmed that these constructs significantly decreased the levels of MCM10 at both the RNA
307 and protein levels relative to the control (shCtrl) (Fig. 6d, e). An *in vitro* limiting dilution assay
308 revealed that *MCM10* depletion with shRNA decreased the tumor sphere-forming ability and
309 estimated CSC frequency (Supplementary Fig. 3g). We then examined the tumor-initiating
310 capacity using a patient-derived xenograft model. Using the *in vivo* limiting dilution assay, we
311 found that *MCM10*-depleted cells had greatly reduced tumor-initiating ability and estimated CSC
312 frequency (Fig. 6f). The tumor growth rate following inoculation of 10^5 cells was also decreased
313 by *MCM10* depletion (Fig. 6g, h). Together, these results illustrate the importance of MCM10 in
314 the maintenance of CSCs *in vitro* and *in vivo*.

315

316 **Expression of c-Myc and MCM10 is enriched in paclitaxel-resistant CSCs that are**
317 **dependent on MCM10 for their maintenance**

318 Finally, we examined the possibility that *MCM10* depletion can eradicate CSCs. CSCs are
319 enriched after paclitaxel treatment, as only differentiated cancer cells are efficiently killed by this
320 chemotherapeutic drug (Y. Li, Atkinson, & Zhang, 2017; Samanta, Gilkes, Chaturvedi, Xiang, &
321 Semenza, 2014). Indeed, when we treated cells with paclitaxel, the remaining resistant cells
322 showed significantly higher sphere-forming abilities (Fig. 7a, b). In addition, we found that the

323 expression levels of MCM10, c-Myc, and Nanog were enriched after treatment (Fig. 7c). However,
324 when *MCM10* was depleted, the paclitaxel-resistant cells displayed a great reduction in sphere-
325 forming abilities, and the enrichment of CSCs with high Nanog and c-Myc expression was
326 abrogated (Fig. 7c, d). These results are consistent with the notion that CSCs that are resistant to
327 paclitaxel can be eradicated by depletion of *MCM10*.

328 Taken together, our findings suggest that upregulated c-Myc increases RNA transcription in
329 CSCs (Fig. 7e). The increased RNA transcription may result in collisions between transcription
330 and replication machinery, thereby causing DNA replication stress, which is more frequent in
331 CSCs than in differentiated cancer cells. Then, MCM10 may activate the dormant origins near
332 the stalled replication forks. Upregulated MCM10 by c-Myc may robustly compensate for DNA
333 replication stress by activating the dormant origins. Therefore, MCM10 is essential for the
334 proliferation of cancer cells and maintenance of CSCs that are resistant to paclitaxel.

335

336 **Discussion**

337 In this study, we provide evidence that a component of the DNA replication initiation machinery,
338 MCM10, is essential for maintaining CSCs, probably by helping them compensate for DNA
339 replication stress. MCM10 expression is upregulated in many types of cancer cells (Cui, Hu, Ning,
340 Tan, & Tang, 2018; W. M. Li et al., 2016; Mahadevappa et al., 2018). Although previous studies
341 reported that MCM10 upregulation is correlated with tumor malignancy, the molecular
342 mechanisms remain largely unclear. We have provided mechanistic insight into how MCM10 is
343 required in cancer cells, including CSCs. MCM10 is likely to efficiently activate dormant origins
344 to compensate for DNA replication stress, which is more frequent in CSCs than in differentiated
345 cancer cells. In contrast, the fact that depletion of MCM10 did not significantly alter cell
346 proliferation in normal cells indicates that a small amount of MCM10 is sufficient for DNA
347 replication in normal cells. In cancer cells, an increased amount of MCM10 appears to be required
348 to compensate for the increased DNA replication stress. Targeting MCM10 will likely be effective

for eliminating cancer cells, including CSCs, without adverse effects on normal cells.

We also show evidence that the replication stress in breast cancer cells and CSCs may be caused by collisions between the transcription and replication machinery. In neural progenitor cells and glioblastoma CSCs, transcription of long neural genes increases the frequency of collisions between the transcription and replication machinery, leading to a higher level of DNA replication stress (Carruthers et al., 2018). On the other hand, in breast CSCs, it appears that upregulated c-Myc induces the collisions between the transcription and replication machinery. Emerging evidence indicates that CSCs are maintained by unique mechanisms that may endow them with a stress-resistant phenotype relative to differentiated cancer cells. CSCs may need to produce a higher amount of proteins than differentiated cancer cells to keep their properties, possibly explaining why CSCs upregulate c-Myc expression. A better understanding of the more detailed mechanisms of replication stress in CSCs will facilitate the development of therapeutic strategies targeting CSCs.

MCM10 was the most highly upregulated gene among the DNA replication initiation factors in spheroid cells compared to adherent cells. We found that other MCMs in the pre-RCs were also among the top 100 upregulated genes. MCM5 was the 43rd most highly upregulated gene and the second most highly upregulated MCM family gene. However, MCM5 depletion did not significantly affect cell proliferation with or without treatment with HU (Supplementary Figure 3b, f) (Woodward et al., 2006). Thus, MCM10 but not MCM5 is likely essential for cancer cell proliferation. In fact, MCM2-7 helicase complexes are expressed abundantly, and cancer cells can survive after depletion of these molecules for some time (Ge et al., 2007). MCM5 remains in the pre-RCs in the licensed or dormant origins, whereas MCM10 is recruited as a firing factor to activate the origins. This functional difference between these MCMs may explain the respective phenotypes in cancer cells after knockdown of each molecule. GINS and CDC45, other firing factors, were the 12^{th} and 19^{th} most highly upregulated genes, respectively, and their roles in CSCs remain unknown. We are interested in analyzing their roles in a future project.

We provide a proof-of-principle that molecules that inhibit functions of MCM10 will be useful for targeting not only cancer cells but also CSCs. Suramin, an anti-parasitic agent, inhibits functions of MCM10 (Paulson et al., 2019). Development of inhibitors of MCM10 without enzymatic activity using Proteolysis Targeting Chimera (PROTAC) technology may be possible (An & Fu, 2018). Furthermore, the combination of such MCM10 inhibitors with chemotherapeutic reagents that induce DNA replication stress is expected to synergistically target cancer cells.

Materials and Methods

Cell lines and cell culture

Breast cancer cell lines MCF7, BT20 and BTB474 were purchased from the American Type Culture Collection (ATCC). Cells were cultured in RPMI1640 (GIBCO, Waltham, MA) supplemented with 10% fetal bovine serum (FBS; GIBCO) and 1% penicillin–streptomycin (P/S; Nacalai tesque, Inc., Kyoto, Japan). HEK293T cells (ATCC) were cultured for virus production in Dulbecco's Modified Eagle Medium: Nutrient Mixture (DMEM) (GIBCO) supplemented with 10% FBS and 1% P/S. The cells were maintained in a humidified incubator with 5% CO_2 at 37°C. They are routinely tested for contamination of mycoplasma by using PCR Micoplasma Test Kit (Takara Bio Inc., Shiga, Japan) and confirmed to be negative before performing experiments.

Primary Cell Culture

To isolate lineage-negative (Lin^-) breast cancer cells, cells obtained from breast tumor specimens were incubated with a mixture of biotin-conjugated antibodies against Lin^+ cells, as previously described (Tominaga et al., 2019). The antibody mixture included a magnetic cell separation (MACS) lineage kit for depletion of hematopoietic and erythrocyte precursor cells (CD2, CD3, CD11b, CD14, CD15, CD16, CD19, CD56, CD123, and CD235a; Miltenyi Biotec, Birgisch Gladbach, Germany), endothelial cells (CD31, eBioscience, San Diego, CA), and stromal cells (CD140b, Biolegend, San Diego, CA). After incubation, cells were separated using the MACS system (Miltenyi Biotec). Isolated Lin^- breast cancer cells were cultured in Human EpiCult™-B Medium Kit medium (Stem Cell Technologies, Vancouver, Canada) containing a supplement mix, freshly prepared 0.48 μg/ml hydrocortisone (Stem Cell Technologies), 2 mM L-glutamine (Nacalai Tesque), 100 units/ml penicillin (Nakarai tesque, Inc.), and 100 μg/ml streptomycin (Nakarai tesque, Inc.). Isolated single cells were cultured in a humidified atmosphere at 37°C in 5% CO_2, and the culture medium was changed every 2 days.

Tumor spheres were cultured as follows. Single-cell suspensions were cultured in ultra-low

attachment plates and cells were grown in SCM, which consists of DMEM/F-12 (GIBCO), 20 ng/mL epidermal growth factor (Millipore, Burlington, MA), 20 ng/mL basic fibroblast growth factor (PeproTech, Cranbury, NJ), B27 supplement (GIBCO), and 2 μg/mL heparin (Stem Cell Technologies), as previously described (Tominaga et al., 2019). Adherent cells attached to regular cell culture plates were cultured in RPMI1640 (GIBCO) supplemented with 10% FBS (GIBCO) and 1% P/S (Nacalai Tesque Inc.). Patient-derived ovarian cancer spheroid cells (OVN62) were established from clinical specimens by the procedures as previously reported (Ishiguro et al., 2016).

Tumor sphere formation assay

We previously confirmed that patient-derived breast cancer cells plated at 5,000 cells/mL yield tumor spheres clonally derived from single cells (Hinohara et al., 2012). Hence, cells were plated as single-cell suspensions on ultra–low-attachment 24-well plates (1000–5000 cells/well) to obtain single cell–derived tumor spheres. The cells were grown in SCM. Spheres with diameter >75 μm were counted after 4–7 days.

Generation of ovarian cancer spheroid cells with inducible-CRISPR/Cas9 targeting *MCM10*

Inducible-Cas9 lentiviral plasmid (Edit-R Inducible lentiviral Cas9; CAS11229) were purchased from Horizon Discovery (Cambridge, UK). For production of lentivirus encoding inducible-Cas9 nuclease, the lentiviral plasmids and packaging plasmids were transfected into lentiX-293T cells using Lipofectamine 2000 (Invitrogen, Carlsbud, CA) and lentivirus-containing supernatants were harvested after 3 days. The lentivirus-containing media was transferred onto OVN62 cells (Ovarian cancer spheroid cells) to generate cells expressing inducible-Cas9 and incubated with blasticidin (5 μ g/mL) (Nakarai tesque, Inc.) for 3 days. After selection, OVN62 cells heterogeneously expressing inducible-Cas9 were performed single-cell sorting using a FACS Aria Ⅲ Cell Sorter (BD Bioscience, San Jose, CA) to pick up stably expressing inducible-Cas9

435 construct.

436 We performed a modification of pLenti-sgRNA plasmid (Addgene #71409) with the sgRNA
437 scaffold with the sgRNA sequence targeting *MCM10* (MCM10 sgRNA #1: 5'-
438 CGGTGAATCTTATACAGAAG-3', MCM10 sgRNA #2: 5'-GAGGGTGGCTCGAACACCAA-
439 3', MCM10 sgRNA #3: 5'-CGGTGAATCTTATACAGAAG-3' and 5'-
440 GAGGGTGGCTCGAACACCAA-3'). OVN62 with stably expressing inducible-Cas9 and
441 targeting *MCM10* were selected by puromycin selection (2 μg/mL) (Nacalai tesque, Inc.).

442

443 **Cell viability assay for ovarian cancer spheroid cells**

444 OVN62 cells stably expressing inducible-Cas9 nuclease and *MCM10*-targeting sgRNA (Non-
445 target sgRNA, MCM10 sgRNA #1, and #2) were treated with Doxycycline (Dox) (Nacalai tesque,
446 Inc.) for 3 days to express Cas9 and induce *MCM10* knockout. After DOX treatment, cells were
447 dissociated to single cells and seeded 3000 cells in each well of the 96-well plates. After 0, 3, 7
448 days incubation, cell viability was measured by using CellTiter-Glo Assay (Promega, Madison,
449 WI).

450

451 **RNA extraction, cDNA amplification, library preparation, and sequencing**

452 Total RNA was extracted from cells using the NucleoSpin RNA XS kit (Clontech, Moutain View,
453 CA). The Smarter Ultra low RNA input kit (Clontech) was used for the synthesis and
454 amplification of cDNA using up to 10 ng of total RNA following the manufacturer's instructions
455 and performing no more than 12 cycles of PCR in order to minimize amplification biases. The
456 quality of cDNA was verified by Agilent 2100 Bioanalyzer using High Sensitivity DNA Chips
457 (Agilent Technologies, Santa Clara, CA). Truseq DNA Illumina libraries were prepared and
458 sequenced to obtain approximately 90 million reads (101 bp paired-end reads) per library using
459 the Hiseq 2000/2500 Illumina sequencer (San Diego, CA).

460

RNA-sequence data analysis

Sequences were trimmed to remove adaptors and low-quality bases. Trimmed reads were mapped onto the hg19 genome (UCSC human genome 19, version:20150519) using Tophat 2.0.10 and transcripts were assembled by Cufflinks 2.1.1 based on RefSeq gene annotation. Transcript expression levels were quantified by Cuffdiff 2.1.1 using the fragments per kilobase of transcript per million mapped fragments (FPKM) method.

GEO accession number is GSE127264.

Real-time PCR analysis

Total RNAs were extracted using TRIzol Reagent (Thermo Fisher Scientific, Waltham, MA) according to the manufacturer's instructions. The High-Capacity cDNA Reverse Transcription Kit (Thermo Fisher Scientific) was used to prepare the cDNA solution. For real-time PCR analyses, Taqman probes of *RPF1*, *LTV1*, *ESF1*, *NSA2*, *BRIX1*, *FCF1*, *MCM10* and *Nanog* were purchased from Applied Biosystems. For detecting premature RNA, primer sequences designed by Kofuji et al. (Kofuji et al., 2019) (pre-rRNA F; 5'-TGTCAGGCGTTCTCGTCTC-3', pre-rRNA R; 5'-AGCACGACGTCACCACATC-3') were used. Reactions were performed using the pre-set program of the ABI ViiA 7 Real-Time PCR System (Thermo Fisher Scientific).

siRNA

We purchased two different siRNA duplexes of *MCM10* (#1, HSS124480 and #2, HSS124482), two different siRNA duplexes of *Myc* (#1, VHS40785 and #2, VHS40789) and a nonspecific control siRNA duplex with similar GC content (siCtrl; Medium GC Duplex #2) from Invitrogen. siRNAs against *MCM5* were designed according to a previous report (Ge et al., 2007); target sequences were 5'-GGAGGUAGCUGAUGAGGUGTT-3' (#1) and 5'-AAGCAGUCGCAGUGAAGAUUG-3' (#2). siRNAs were transfected using RNAiMAX (Invitrogen).

Transient overexpression of MCM10

Cells were transfected with pCMV6-Myc-DDK-MCM10 (OriGene, Rockville, MD) and control vector using ViaFect Transfection Reagent (Promega, Madison, WI).

Western blot analysis

Immunoblotting was performed using standard procedures as described (Hinohara et al., 2012). Antibodies against Nanog (4903S), Oct-4 (2750S), ATR (2790S), p-ATR (2853S), Chk1 (2360T), p-Chk1 (2349T), c-Myc (5605S) and Myc-tag (2278) were purchased from Cell Signaling Technology (Danvers, MA). Antibodies against MCM10 (3733) and MCM5 (17967) were purchased from Abcam (Cambridge, UK). Anti-actin antibody (MAB150) was purchased from Millipore. Cas9 antibody was purchased from Active Motif. Proteins were detected with horseradish peroxidase–conjugated anti-mouse or anti-rabbit antibodies (GE Healthcare Life Sciences, Marlborough, MA).

Immunocytochemistry

Cells in adherent and sphere culture condition were plated on BioCoat Culture Slide (Corning, Corning, NY) after trypsinization, and incubated for 6 h. To detect expression of proteins, cells were fixed with 4% paraformaldehyde (PFA) (Wako, Osaka, Japan) or 100% methanol (Wako, Osaka, Japan), 6 h after seeding, the shortest period for cell attachment. Cells were incubated with 0.2% Triton X-100 (Wako, Osaka, Japan) to permeabilize membranes, and stained overnight with primary antibodies and for 1 h with secondary antibodies. Immunofluorescent visualization of Nuclei was counterstained with DAPI (Thermo Fisher Scientific). Coverslips were mounted with Fluorescence Mounting Medium (Dako, Glostrup, Denmark). Immunofluorescence was detected using an Olympus IXplore pro microscope (Tokyo, Japan) or Nikon confocal microscopy (A1 HD25) (Tokyo, Japan) with the ANDOR software. Acquired images were analyzed by ImageJ

513 software. Antibodies against Nanog (4903S) and c-Myc (5605S) were purchased from Cell
514 Signaling Technology. MCM10 antibody was purchased from Invitrogen (PA5-67218). S9.6
515 antibody that binds to RNA/DNA hybrid was purchased from Millipore (MABE1095).
516
517 **RNaseH treatment**
518 Cells were incubated with Ribonuclease H RNaseH (60 U/μl) (Takara Bio Inc., Code No. 2150A)
519 for 4 hours before immunocytochemistry assay.
520
521 **Proliferation assay for breast cancer cells**
522 Cells were seeded in 12-well plates at low density (5000–10000 cells/well), cultured in
523 RPMI1640 supplemented with 10% FBS and 1% P/S or DMEM with 10% FBS and 1% P/S. HU
524 (Wako, Tokyo, Japan) was added to the medium as necessary. After 4–6 days, cells were harvested
525 and counted.
526
527 **Flow cytometry analysis**
528 To identify the breast CSC population, cells were stained with Alexa Fluor 647–conjugated anti–
529 human CD24 and APC-H7 labeled anti–human CD44 antibodies (BD Pharmingen, San Jose, CA)
530 at 4°C for 20 min. The cells were then analyzed with a FACSAria II flow cytometer (BD
531 Bioscience, San Jose, CA). Dead cells were excluded by propidium iodide (PI; Sigma, St. Luis,
532 MO) staining. Data were analyzed using the FlowJo software (TreeStar, San Carlos, CA).
533 To detect DNA-binding MCM3, collected cells were first treated with 750 μL low-salt
534 extraction buffer (0.1% Igepal CA-630, 10 mM NaCl, 5 mM $MgCl_2$, 0.1 mM PMSF, 10 mM
535 potassium phosphate buffer [pH 7.4]) for 5 min on ice. Then, the cells were fixed by adding 250
536 μL 10% formalin (SIGMA). After incubation at 4°C for 1 h, the cells were washed with phosphate
537 buffered saline (PBS)(GIBCO). Extracted cells were then incubated with anti-MCM3 antibody
538 (Abcam) and anti–rabbit IgG secondary antibody (Alexa Fluor 488) (Molecular Probes, Eugene,

539 OR) in flow buffer (0.1% Igepal CA-630, 6.5 mM Na_2HPO_4, 1.5 mM KH_2PO_4, 2.7 mM KCl, 137
540 mM NaCl, 0.5 mM EDTA [pH 7.5]). Cells were analyzed on a FACSAria II flow cytometer (BD
541 Bioscience) after staining with Hoechst 33258 (Sigma) to detect nuclear DNA (1 μg/mL).
542
543 **DNA fiber assay**
544 Adherent and sphere-cultured cells were pulsed-labeled with 25 μM ldU (Sigma) for 30 min,
545 followed by 250 μM CIdU (Sigma) for 30 min. The cells were trypsinized and resuspended in
546 100 μL PBS (GIBCO)(10^5–10^6 cells/mL). Then, a 2 μL cell suspension was placed at the end of
547 a glass slide. After air drying for 8 min, 7 μL of fiber lysis solution (50 mM EDTA, 0.5% SDS,
548 200 mM Tris-HCl [pH 7.5]) was pipetted on top of the cell suspension and mixed. Cell lysis
549 proceeded for 5 min, and then the slides were tilted at 15° to allow the DNA spread down the
550 slide. Slides were air-dried for 15 min and fixed in methanol/acetic acid (3:1). After washing with
551 distilled water, DNA was denatured in 2.5 M HCl for 80 min. The slides were washed with PBS
552 three times, and blocked for 1 h in 5% bovine serum albumin (BSA) (Sigma) in PBS (GIBCO).
553 After blocking, the slides were incubated with primary antibodies (anti-CldU, Abcam ab6326;
554 anti-IdU, BD 347580) followed by secondary antibodies (Alexa Fluor 594–conjugated anti–rat
555 IgG and Alexa Fluor 488–conjugated anti–mouse IgG)(Molecular Probes).
556
557 **Plasmid construction**
558 The pLKO shRNA vector was used for knockdown experiments. Target sequences for human
559 *MCM10* were 5'-TCATCCTCAGAAGGTCTTAAT-3' (#1) and 5'-
560 GGACTTAACAGATGAAGAAGA-3' (#2). Lentiviral plasmids were transduced into HET293T
561 cells along with ViraPower Lentiviral Packaging Mix (Invitrogen) using the Lipofectamine 3000
562 Transfection Reagent (Invitrogen). The medium was changed after 16 h.
563
564 **Transduction of patient-derived cancer cells with lentiviral vectors**

Culture supernatant from HEK293T cells containing virus particles was applied to patient-derived cancer cells. The cells were incubated at 37°C in 5% CO_2 for 48 h, and then virus-infected cells were selected using 2.5 μg/mL puromycin for breast cancer cells and 2 μg/mL puromycin (Nakarai tesque, Inc.) for ovarian cancer spheroid cells.

In vivo limiting dilution assay

Seven-week-old female immunodeficient NSG mice were anesthetized with isoflurane (Abbott, Lake Bluff, IL). Patient-derived breast cancer cells infected with lentivirus (shMCM10 #1, #2, and shCtrl), or cells cultured in adherent and sphere condition were suspended in 50 μL Matrigel (BD Biosciences) in a dilution series (10^3, 10^4, and 10^5 cells). Suspended samples were then injected subcutaneously into the mammary fat pads of NSG mice. Tumor volume was measured twice a week using the following formula: $V = 1/2(L \times W^2)$, where L equals length and W equals width. Tumors larger than 50 mm^3 were counted.

Statistical analysis

All data are presented as means ± SEM or means ± SD. The unpaired Student *t*-test was used to compare differences between two samples, and values of $p < 0.01$–0.05 (*), $p < 0.001$–0.01 (**), or $p < 0.001$ (***) were considered significant. Tumor-initiating frequency was calculated using the ELDA Software. Kaplan-Meier survival curves were analyzed by log-rank test.

Study approval

All human breast carcinoma specimens were obtained from The University of Tokyo Hospital, Minami-Machida Hospital and Kanazawa University Hospital. Human ovarian cancer specimens were obtained from Niigata University Medical & Dental Hospital. This study was approved by the institutional review boards of the Institute of Medical Science, The University of Tokyo; The University of Tokyo Hospital; Minami Machida Hospital; National Cancer Center; Niigata

University; and Kanazawa University. Written informed consent was received from all participants before inclusion in the study.

Acknowledgements

We thank H. Nakauchi, Y. Ishii, and A. Fujita for their help with flow cytometry. This work was supported in part by an Extramural Collaborative Research Grant from the Cancer Research Institute, Kanazawa University, a Research Grant from Princess Takamatsu Cancer Research Fund (17-2924), a Grant-in-Aid for Scientific Research from JSPS (17K19587 and 18H02679), and a research grant from AMED Project for Development of Innovative Research on Cancer Therapeutics, Project for Cancer Research and Therapeutic Evolution (16cm0106120h0001) and Practical Research for Innovative Cancer Control (16ck0106194h0001) to N.G. This work was also supported by MEXT KAKENHI (No. 221S0002) to N.G. This work was supported by the Graduate Program for Leaders in Life Innovation (GPLLI) at The University of Tokyo Life Innovation Leading Graduate School (to T.M., http://square.umin.ac.jp/gplli/en/index.html) and a Grant-in-Aid for a Japan Society for Promotion of Science (JSPS) fellowship (to T.M., http://www.jsps.go.jp/english/e-pd/index.html).

Author contributions

T.M. performed experiments, analyzed and interpreted data and wrote the manuscript. Y.T., K.Y., NM.RC., T. Nishimura, Y.K., A.N., K.T. and A.S. performed experiments and analyzed data. T. Natsume and M.T.K. helped fiber assay, analyzed data and provided scientific insight. M.T.K. also wrote the manuscript. M.Y., S.I, M.I., T.O., T.E., M.T. and K.T. provided clinical samples. K.I., K.H-I., S.I. and K.O. analyzed data and provided scientific insight. M.S. and Y.S. performed RNA sequencing and analyzed data. S.S. and A.T. provided scientific insight and supervised the study. N.G. conceived the study, analyzed and interpreted data and wrote the manuscript. All

617 authors read the manuscript and provided feedback on the manuscript.

618

References

Ablett, M. P., Singh, J. K., & Clarke, R. B. (2012). Stem cells in breast tumours: are they ready for the clinic? *Eur J Cancer, 48*(14), 2104–2116. doi:10.1016/j.ejca.2012.03.019

Al-Hajj, M., Wicha, M. S., Benito-Hernandez, A., Morrison, S. J., & Clarke, M. F. (2003). Prospective identification of tumorigenic breast cancer cells. *Proc Natl Acad Sci U S A, 100*(7), 3983–3988. doi:10.1073/pnas.0530291100

An, S., & Fu, L. (2018). Small-molecule PROTACs: An emerging and promising approach for the development of targeted therapy drugs. *EBioMedicine, 36*, 553–562. doi:10.1016/j.ebiom.2018.09.005

Batlle, E., & Clevers, H. (2017). Cancer stem cells revisited. *Nat Med, 23*(10), 1124–1134. doi:10.1038/nm.4409

Baxley, R. M., & Bielinsky, A. K. (2017). Mcm10: A Dynamic Scaffold at Eukaryotic Replication Forks. *Genes (Basel), 8*(2). doi:10.3390/genes8020073

Beier, D., Hau, P., Proescholdt, M., Lohmeier, A., Wischhusen, J., Oefner, P. J., . . . Beier, C. P. (2007). CD133(+) and CD133(-) glioblastoma-derived cancer stem cells show differential growth characteristics and molecular profiles. *Cancer Res, 67*(9), 4010–4015. doi:10.1158/0008-5472.CAN-06-4180

Blow, J. J., & Ge, X. Q. (2009). A model for DNA replication showing how dormant origins safeguard against replication fork failure. *EMBO Rep, 10*(4), 406–412. doi:10.1038/embor.2009.5

Carruthers, R. D., Ahmed, S. U., Ramachandran, S., Strathdee, K., Kurian, K. M., Hedley, A., . . . Chalmers, A. J. (2018). Replication Stress Drives Constitutive Activation of the DNA Damage Response and Radioresistance in Glioblastoma Stem-like Cells. *Cancer Res, 78*(17), 5060–5071. doi:10.1158/0008-5472.CAN-18-0569

Clement, V., Sanchez, P., de Tribolet, N., Radovanovic, I., & Ruiz i Altaba, A. (2007). HEDGEHOG-GLI1 signaling regulates human glioma growth, cancer stem cell self-renewal, and tumorigenicity. *Curr Biol, 17*(2), 165–172. doi:10.1016/j.cub.2006.11.033

Cui, F., Hu, J., Ning, S., Tan, J., & Tang, H. (2018). Overexpression of MCM10 promotes cell proliferation and predicts poor prognosis in prostate cancer. *Prostate*. doi:10.1002/pros.23703

Desmedt, C., Piette, F., Loi, S., Wang, Y., Lallemand, F., Haibe-Kains, B., . . . Consortium, T. (2007). Strong time dependence of the 76-gene prognostic signature for node-negative breast cancer patients in the TRANSBIG multicenter independent validation series. *Clin Cancer Res, 13*(11), 3207–3214. doi:10.1158/1078-0432.CCR-06-2765

Dontu, G., Al-Hajj, M., Abdallah, W. M., Clarke, M. F., & Wicha, M. S. (2003). Stem cells in normal breast development and breast cancer. *Cell Prolif, 36 Suppl 1*, 59–72. Retrieved from https://www.ncbi.nlm.nih.gov/pubmed/14521516

Douglas, M. E., Ali, F. A., Costa, A., & Diffley, J. F. X. (2018). The mechanism of eukaryotic CMG helicase activation. *Nature, 555*(7695), 265–268. doi:10.1038/nature25787

Fragkos, M., Ganier, O., Coulombe, P., & Mechali, M. (2015). DNA replication origin activation in space and time. *Nat Rev Mol Cell Biol, 16*(6), 360–374. doi:10.1038/nrm4002

Gaillard, H., Garcia-Muse, T., & Aguilera, A. (2015). Replication stress and cancer. *Nat Rev Cancer, 15*(5), 276–289. doi:10.1038/nrc3916

Gambus, A., Jones, R. C., Sanchez-Diaz, A., Kanemaki, M., van Deursen, F., Edmondson, R. D., & Labib, K. (2006). GINS maintains association of Cdc45 with MCM in replisome progression

complexes at eukaryotic DNA replication forks. *Nat Cell Biol, 8*(4), 358–366. doi:10.1038/ncb1382

Gan, W., Guan, Z., Liu, J., Gui, T., Shen, K., Manley, J. L., & Li, X. (2011). R-loop-mediated genomic instability is caused by impairment of replication fork progression. *Genes Dev, 25*(19), 2041–2056. doi:10.1101/gad.17010011

Ge, X. Q., Jackson, D. A., & Blow, J. J. (2007). Dormant origins licensed by excess Mcm2–7 are required for human cells to survive replicative stress. *Genes Dev, 21*(24), 3331–3341. doi:10.1101/gad.457807

Hinohara, K., Kobayashi, S., Kanauchi, H., Shimizu, S., Nishioka, K., Tsuji, E., . . . Gotoh, N. (2012). ErbB receptor tyrosine kinase/NF-kappaB signaling controls mammosphere formation in human breast cancer. *Proc Natl Acad Sci U S A, 109*(17), 6584–6589. doi:10.1073/pnas.1113271109

Ishiguro, T., Sato, A., Ohata, H., Ikarashi, Y., Takahashi, R. U., Ochiya, T., . . . Okamoto, K. (2016). Establishment and Characterization of an In Vitro Model of Ovarian Cancer Stem-like Cells with an Enhanced Proliferative Capacity. *Cancer Res, 76*(1), 150–160. doi:10.1158/0008-5472.CAN-15-0361

Kanke, M., Kodama, Y., Takahashi, T. S., Nakagawa, T., & Masukata, H. (2012). Mcm10 plays an essential role in origin DNA unwinding after loading of the CMG components. *EMBO J, 31*(9), 2182–2194. doi:10.1038/emboj.2012.68

Kofuji, S., Hirayama, A., Eberhardt, A. O., Kawaguchi, R., Sugiura, Y., Sampetrean, O., . . . Sasaki, A. T. (2019). IMP dehydrogenase-2 drives aberrant nucleolar activity and promotes tumorigenesis in glioblastoma. *Nat Cell Biol, 21*(8), 1003–1014. doi:10.1038/s41556-019-0363-9

Kotsantis, P., Petermann, E., & Boulton, S. J. (2018). Mechanisms of Oncogene-Induced Replication Stress: Jigsaw Falling into Place. *Cancer Discov, 8*(5), 537–555. doi:10.1158/2159-8290.CD-17-1461

Li, W. M., Huang, C. N., Ke, H. L., Li, C. C., Wei, Y. C., Yeh, H. C., . . . Wu, W. J. (2016). MCM10 overexpression implicates adverse prognosis in urothelial carcinoma. *Oncotarget, 7*(47), 77777–77792. doi:10.18632/oncotarget.12795

Li, Y., Atkinson, K., & Zhang, T. (2017). Combination of chemotherapy and cancer stem cell targeting agents: Preclinical and clinical studies. *Cancer Lett, 396*, 103–109. doi:10.1016/j.canlet.2017.03.008

Looke, M., Maloney, M. F., & Bell, S. P. (2017). Mcm10 regulates DNA replication elongation by stimulating the CMG replicative helicase. *Genes Dev, 31*(3), 291–305. doi:10.1101/gad.291336.116

Macheret, M., & Halazonetis, T. D. (2018). Intragenic origins due to short G1 phases underlie oncogene-induced DNA replication stress. *Nature, 555*(7694), 112–116. doi:10.1038/nature25507

Mahadevappa, R., Neves, H., Yuen, S. M., Jameel, M., Bai, Y., Yuen, H. F., . . . Kwok, H. F. (2018). DNA Replication Licensing Protein MCM10 Promotes Tumor Progression and Is a Novel Prognostic Biomarker and Potential Therapeutic Target in Breast Cancer. *Cancers (Basel), 10*(9). doi:10.3390/cancers10090282

Masai, H., Matsumoto, S., You, Z., Yoshizawa-Sugata, N., & Oda, M. (2010). Eukaryotic chromosome DNA replication: where, when, and how? *Annu Rev Biochem, 79*, 89–130.

doi:10.1146/annurev.biochem.052308.103205

Meyer, N., & Penn, L. Z. (2008). Reflecting on 25 years with MYC. *Nat Rev Cancer, 8*(12), 976–990. doi:10.1038/nrc2231

Murayama, T., Nakaoku, T., Enari, M., Nishimura, T., Tominaga, K., Nakata, A., . . . Gotoh, N. (2016). Oncogenic Fusion Gene CD74–NRG1 Confers Cancer Stem Cell–like Properties in Lung Cancer through a IGF2 Autocrine/Paracrine Circuit. *Cancer Res, 76*(4), 974–983. doi:10.1158/0008–5472.CAN–15–2135

Paulson, C. N., John, K., Baxley, R. M., Kurniawan, F., Orellana, K., Francis, R., . . . Bielinsky, A. K. (2019). The anti–parasitic agent suramin and several of its analogues are inhibitors of the DNA binding protein Mcm10. *Open Biol, 9*(8), 190117. doi:10.1098/rsob.190117

Pawitan, Y., Bjohle, J., Amler, L., Borg, A. L., Egyhazi, S., Hall, P., . . . Bergh, J. (2005). Gene expression profiling spares early breast cancer patients from adjuvant therapy: derived and validated in two population–based cohorts. *Breast Cancer Res, 7*(6), R953–964. doi:10.1186/bcr1325

Petropoulos, M., Champeris Tsaniras, S., Taraviras, S., & Lygerou, Z. (2019). Replication Licensing Aberrations, Replication Stress, and Genomic Instability. *Trends Biochem Sci, 44*(9), 752–764. doi:10.1016/j.tibs.2019.03.011

Pettitt, S. J., & Lord, C. J. (2019). Dissecting PARP inhibitor resistance with functional genomics. *Curr Opin Genet Dev, 54*, 55–63. doi:10.1016/j.gde.2019.03.001

Ponti, D., Costa, A., Zaffaroni, N., Pratesi, G., Petrangolini, G., Coradini, D., . . . Daidone, M. G. (2005). Isolation and in vitro propagation of tumorigenic breast cancer cells with stem/progenitor cell properties. *Cancer Res, 65*(13), 5506–5511. doi:10.1158/0008–5472.CAN–05–0626

Samanta, D., Gilkes, D. M., Chaturvedi, P., Xiang, L., & Semenza, G. L. (2014). Hypoxia–inducible factors are required for chemotherapy resistance of breast cancer stem cells. *Proc Natl Acad Sci U S A, 111*(50), E5429–5438. doi:10.1073/pnas.1421438111

Sansone, P., Storci, G., Tavolari, S., Guarnieri, T., Giovannini, C., Taffurelli, M., . . . Bonafe, M. (2007). IL–6 triggers malignant features in mammospheres from human ductal breast carcinoma and normal mammary gland. *J Clin Invest, 117*(12), 3988–4002. doi:10.1172/JCI32533

Saygin, C., Matei, D., Majeti, R., Reizes, O., & Lathia, J. D. (2019). Targeting Cancer Stemness in the Clinic: From Hype to Hope. *Cell Stem Cell, 24*(1), 25–40. doi:10.1016/j.stem.2018.11.017

Schwab, R. A., & Niedzwiedz, W. (2011). Visualization of DNA replication in the vertebrate model system DT40 using the DNA fiber technique. *J Vis Exp*(56), e3255. doi:10.3791/3255

Techer, H., Koundrioukoff, S., Nicolas, A., & Debatisse, M. (2017). The impact of replication stress on replication dynamics and DNA damage in vertebrate cells. *Nat Rev Genet, 18*(9), 535–550. doi:10.1038/nrg.2017.46

Tominaga, K., Minato, H., Murayama, T., Sasahara, A., Nishimura, T., Kiyokawa, E., . . . Gotoh, N. (2019). Semaphorin signaling via MICAL3 induces symmetric cell division to expand breast cancer stem–like cells. *Proc Natl Acad Sci U S A, 116*(2), 625–630. doi:10.1073/pnas.1806851116

Torre, L. A., Bray, F., Siegel, R. L., Ferlay, J., Lortet–Tieulent, J., & Jemal, A. (2015). Global cancer statistics, 2012. *CA Cancer J Clin, 65*(2), 87–108. doi:10.3322/caac.21262

van Deursen, F., Sengupta, S., De Piccoli, G., Sanchez–Diaz, A., & Labib, K. (2012). Mcm10 associates with the loaded DNA helicase at replication origins and defines a novel step in its activation. *EMBO J, 31*(9), 2195–2206. doi:10.1038/emboj.2012.69

749 Vesela, E., Chroma, K., Turi, Z., & Mistrik, M. (2017). Common Chemical Inductors of Replication
750 Stress: Focus on Cell-Based Studies. *Biomolecules, 7*(1). doi:10.3390/biom7010019
751 Vijayraghavan, S., Tsai, F. L., & Schwacha, A. (2016). A Checkpoint-Related Function of the MCM
752 Replicative Helicase Is Required to Avert Accumulation of RNA:DNA Hybrids during S-phase
753 and Ensuing DSBs during G2/M. *PLoS Genet, 12*(8), e1006277.
754 doi:10.1371/journal.pgen.1006277
755 Wasserman, M. R., Schauer, G. D., ODonnell, M. E., & Liu, S. (2019). Replication Fork Activation Is
756 Enabled by a Single-Stranded DNA Gate in CMG Helicase. *Cell, 178*(3), 600-611 e616.
757 doi:10.1016/j.cell.2019.06.032
758 Watase, G., Takisawa, H., & Kanemaki, M. T. (2012). Mcm10 plays a role in functioning of the
759 eukaryotic replicative DNA helicase, Cdc45-Mcm-GINS. *Curr Biol, 22*(4), 343-349.
760 doi:10.1016/j.cub.2012.01.023
761 Woodward, A. M., Gohler, T., Luciani, M. G., Oehlmann, M., Ge, X., Gartner, A., . . . Blow, J. J. (2006).
762 Excess Mcm2-7 license dormant origins of replication that can be used under conditions of
763 replicative stress. *J Cell Biol, 173*(5), 673-683. doi:10.1083/jcb.200602108
764 Zeman, M. K., & Cimprich, K. A. (2014). Causes and consequences of replication stress. *Nat Cell Biol,*
765 *16*(1), 2-9. doi:10.1038/ncb2897
766 Zhang, Y., & Weinberg, R. A. (2018). Epithelial-to-mesenchymal transition in cancer: complexity and
767 opportunities. *Front Med, 12*(4), 361-373. doi:10.1007/s11684-018-0656-6
768

Figure legends

Figure 1. CSCs are enriched in sphere culture population and show activation of distinct pathways and c-Myc expression is upregulated in CSC-enriched spheroid cells

a, Images of PDC #1 cultured in adherent condition (adh; left), and in sphere culture condition (sph; right) are shown. Scale bar = 100 μm. **b**, Results of limiting dilution assay of PDC#1 obtained under adherent and sphere culture conditions were compared. CSC frequency and p-value were determined using the ELDA software (http://bioinf.wehi.edu.au/software/elda/index.html). **c,** Expression levels of MCM10 and Nanog in MCF7 and PDC #1 cells were compared between cells cultured under adherent and sphere conditions. Actin was used for loading control. **d**, (Left) Immunofluorescence images of Nanog staining in PDC #1 cells cultured under adherent and sphere conditions are shown. Nuclei were counterstained with DAPI. Arrows indicate cells with strong Nanog staining. Scale bar = 50 μm. (Right) The intensities of Nanog staining were quantified by using ImageJ software. One hundred cells in each slide were counted (mean ±SD, n = 3; ***$p < 0.001$). **e**, PDC #1 cells obtained by adherent and sphere culture conditions were stained with CD44 and CD24 antibodies, and then subjected to flow cytometry analysis. **f**, Schematic of the experimental procedure. Cancer cells were separated from clinical breast tumor samples, and then they were cultured in adherent and sphere conditions. RNAs were collected from both two conditions for RNA-seq transcriptome analysis. **g**, Gene set enrichment analysis (GSEA) was used to compare gene expression profiles of PDC #1-#3. Gene sets related to Drug resistance (KANG DOXORUBICIN RESISTANCE UP), EMT (SARRIO EPITHELIAL MESENCHYMAL TRANSITION UP), Myc targets (YU MYC TARGETS UP) and Replication stress response (REACTOME ACTIVATION OF ATR IN RESPONSE TO REPLICATION STRESS) were upregulated in the sphere population. NES; normalized enrichment score, FDR; false discovery ratio. **(h)** Expression level of c-Myc in PDC #1, #4 and #6 as determined by immunoblotting, were compared between cells cultured in the adherent and sphere conditions. Actin was used for loading control. **(i)** (Left)

795 Immunofluorescence images of c-Myc staining in PDC #1 cells cultured in the adherent and
796 sphere conditions are shown. Nuclei were counterstained with DAPI. Arrows indicate cells with
797 strong c-Myc staining. Scale bar = 50 μm. (Right) The intensities of c-Myc staining were
798 quantified by using ImageJ software. One hundred cells in each slide were counted (mean ±SD,
799 n = 3; ***p < 0.001). **c, h**, Immunoblotting experiments were independently performed 3 times
800 and representative results were presented.
801
802 **Figure 2. c-Myc expression and DNA replication stress are upregulated in CSC-enriched**
803 **spheroid cells**
804 **a,** Expression levels of ATR, p-ATR, Chk1 and p-Chk1 as determined by immunoblotting, were
805 compared between cells cultured in the adherent and sphere conditions. Expression was quantified
806 by ImageJ and normalized to Actin. The exposure time was adjusted so that the intensities of the
807 bands were within the linear range. Experiments were independently performed 3 times and
808 representative results were presented. **b**, Schematic of the experimental procedure. Cells were
809 incubated sequentially with IdU then CldU. Labeled DNA was spread on glass slides, and then
810 stained with antibodies for IdU (green) and CldU (red). If replication started in the first 30 min,
811 bidirectional forks stained with green and red could be observed. **c**, Proportion of asymmetric
812 forks, representative of replication stress. The ratio of longer CldU tracks (L1) to shorter tracks
813 (L2) was calculated; forks with L1/L2 ≥ 1.3 were regarded as asymmetric. Thirty bidirectional
814 forks in each slide were counted. Three slides for each population were prepared (mean ± SEM,
815 n = 3; *p < 0.05). Scale bar = 10 μm. **d**, Proportion of stalled forks, labeled only with green was
816 calculated. Two hundred labeled forks in each slide were counted. Three slides for each population
817 were prepared (mean ± SEM, n = 3; **p < 0.01). Scale bar = 5 μm. **e**, Immunofluorescence images
818 of RNA/DNA hybrid staining in PDCs were shown. Cells were cultured in the adherent condition
819 with or without RNaseH treatment. Nuclei were counterstained with DAPI. Scale bar = 10 μm. **f**,
820 (Left) Immunofluorescence images of RNA/DNA hybrid staining in PDCs cultured in the

821 adherent and sphere conditions are shown. (Right) Number of RNA/DNA hybrid foci in each cell
822 was counted and compared between the two conditions. Hundred cells in each slide were counted.
823 Three slides for each population were prepared (mean ± SEM, n = 3; ***p < 0.001).
824
825 **Figure 3. c-Myc expression contributes to replication stress**
826 **a**, Knockdown efficiencies of siRNAs targeting *c-Myc* (siMyc #1 and #2) or control siRNA
827 (siCtrl) in PDCs was compared by immunoblotting (left) and qPCR (right) (mean ± SEM, n = 3;
828 ***p < 0.001). **b**, Number of RNA/DNA hybrid foci in each cell was counted and compared
829 among spheroid cells treated with siCtrl, *siMyc* #1, and *siMyc* #2. Scale bar = 10 μm. Hundred
830 cells in each slide were counted. Three slides for each population were prepared (mean ± SEM, n
831 = 3; ***p < 0.001). **c**, Expression levels of ATR, p-ATR, Chk1 and p-Chk1 as determined by
832 immunoblotting, were compared among cells treated with siCtrl, *siMyc* #1, and *siMyc* #2.
833 Expression was quantified by ImageJ and normalized to Actin. **a,c**, Immunoblotting experiments
834 were independently performed 3 times and representative results were presented.
835
836 **Figure 4. MCM10 expression is upregulated in CSC-enriched spheroid cells and MCM10 is**
837 **co-localized with RNA/DNA hybrid foci**
838 **a,** Expression levels of MCM10 in MCF10A, MCF7, BT20, and BT474 were compared by
839 immunoblotting. Actin was used for loading control. **b**, Expression level of MCM10 in PDCs
840 treated with siCtrl, *siMyc* #1 and *siMyc* #2 was compared by immunoblotting (left) and qPCR
841 (right) (mean ± SEM, n = 3; ***p < 0.001). Actin was used for loading control. **c**, Expression
842 levels of *MCM10* in PDC #1, #4, #5 and MCF7 cells were compared between cells cultured in
843 the adherent and sphere conditions, by qPCR (mean ± SEM, n = 3; ***p < 0.001, **p < 0.01). **d**,
844 Expression levels of MCM10 were compared in cells cultured in the adherent and sphere
845 conditions, by immunoblotting. Actin was used for loading control. **e**, Immunofluorescence
846 images of MCM10 staining in PDCs after transfection with control siRNA (left) or *siMCM10* #1

(right) are shown. Nuclei were counterstained with DAPI. Scale bar = 5 μm. Experiments were independently performed 3 times and representative results were presented. **f,** (left) Immunofluorescence images of MCM10 staining in PDCs cultured in the adherent and sphere conditions are shown. Nuclei were counterstained with DAPI. Scale bar = 50 μm. (right) The intensities of c-Myc staining were quantified by using ImageJ software. One hundred cells in each slide were counted (mean ±SD, n = 3; ***p < 0.001). **g**, (Left) Immunofluorescence images of MCM10 and S9.6 antibody staining in PDCs cultured in the sphere conditions are shown. The median values of the intensities of MCM10 staining (**f**) were used as the cut-off to determine MCM10-low cells and MCM10-high cells. Nuclei were counterstained with DAPI. Arrowheads indicate double positive puncta. Scale bar = 5 μm. (Right) Scatter plot showing total number of MCM10-positive puncta and double positive puncta in each cell. MCM10-positive puncta and double positive puncta were quantified by using ImageJ software. Fifty cells were counted for each group. (mean ± SD; ***p < 0.001). **a,b,d**, Immunoblotting experiments were independently performed 3 times and representative results were presented.

Figure 5. MCM10 plays important roles for proliferation of cancer cells

a, Kaplan–Meier survival curves were drawn using the Stockholm cohort (GSE1456; overall survival) and the Uppsala, Oxford, Stockholm, IGR, GUYT, and CRH cohorts (GSE7390; overall survival). The median values were used as the cut-off. P-values were obtained by log-rank test. **b,c**, Knockdown efficiencies of siRNAs targeting *MCM10* (siMCM10 #1 and #2) in MCF7, BT20 and PDC #1, and DOX-inducible knockout in PDC #8 were compared by immunoblotting (**b**) and qPCR (**c**) (mean ± SEM, n = 3; ***p < 0.001). Immunoblotting experiments were independently performed 3 times and representative results were presented. **d**, Cells were seeded in 12-well plates (10,000 cells/well) and cultured. Then they were harvested and counted after 4 days (mean ± SEM, n = 3; **p < 0.01, *p < 0.05). **e**, (Left) PDCs treated with siCtrl, *siMCM10* #1, or *siMCM10* #2 were incubated with BrdU for 30 min. DNA and incorporated BrdU content were

873 analyzed by flow cytometry. (Right) Proportion of BrdU positive cells was averaged from three
874 biological replicates (mean ± SEM, n = 3; ***p < 0.001, **p < 0.01).
875
876 **Figure 6. MCM10 plays important roles for CSC properties**
877 **a**, (Left) Representative images of tumor spheres. PDC #1, #7 and MCF7 cells treated with siRNA
878 targeting *MCM10* and DOX-inducible *MCM10* knockout PDC #8 cells were cultured under
879 sphere conditions. Scale bar = 100 μm. (Right) Quantification of tumor sphere formation
880 efficiency. Spheres were formed for 6 days (mean ± SEM, n = 4; ***p < 0.001, **p < 0.01, *p <
881 0.05). **b**, MCF7 and BT20 cells treated with siCtrl, *siMCM10* #1 or *siMCM10* #2 were stained
882 with CD44 and CD24 antibodies, and then subjected to flow cytometry analysis. **c**, Expression
883 levels of Nanog and Oct-4, as determined by immunoblotting, were compared between PDCs
884 treated with siCtrl, *siMCM10* #1 and *siMCM10* #2. **d**, Expression level of *MCM10* was analyzed
885 by qPCR in PDCs introduced with shCtrl, *shMCM10* #1, or *shMCM10* #2 (mean ± SEM, n = 3;
886 ***p < 0.001). **e**, Expression levels of MCM10 and Nanog were compared by immunoblotting in
887 PDCs introduced with shCtrl, *shMCM10* #1, or *shMCM10* #2. **f**, Results of limiting dilution assay
888 of shRNA-introduced PDCs #1 were shown. Tumors larger than 50 mm^3 were counted. CSC
889 frequency and p-values were determined using the ELDA software. **g,h**, Growth curves (**g**) and
890 representative images (**h**) of tumors are shown (1×10^5 cells/site). Scale bar = 10 mm. **c,e**,
891 Immunoblotting experiments were independently performed 3 times and representative results
892 were presented.
893
894 **Figure 7. Paclitaxel-resistant cancer cells are dependent on MCM10 for their maintenance**
895 **a**, PDCs were seeded in 12-well plates (10,000 cells/well) and cultured with 10 nM paclitaxel or
896 control DMSO for 3 days. Cells were harvested and counted (mean ± SEM, n = 3; ***p < 0.001).
897 **b**, Those survived cells after the treatment with paclitaxel or DMSO were used for analyzing
898 sphere forming ability. Spheres were counted after 6 days (mean ± SEM, n = 4; **p < 0.01). **c,d**,

The survived cells after the treatment with paclitaxel or DMSO were treated with siRNA for *MCM10* or control siRNA (Ctrl), and then cultured in the sphere conditions. Expression levels of Nanog, c-Myc and MCM10, as determined by immunoblotting, were compared (**c**). Expression was quantified by ImageJ and normalized to Actin. The exposure time was adjusted so that the intensities of the bands were within the linear range. Experiments were independently performed 3 times and representative results were presented. **d,** Representative images of tumor spheres are shown (upper panels). Scale bar = 100 μm. Spheres were counted after 4 days (mean ± SEM, n = 4; ***p < 0.001, **p < 0.01) (lower panel). **e**, Models of MCM10 function in CSCs and differentiated cancer cells are illustrated. In CSCs, upregulation of c-Myc leads to higher level of replication stress due to collisions between transcription machinery and replication machinery. MCM10 is necessary to deal with such DNA replication stress. MCM10 promotes completion of DNA replication by activating dormant origins near the stalled forks.

Figure 1

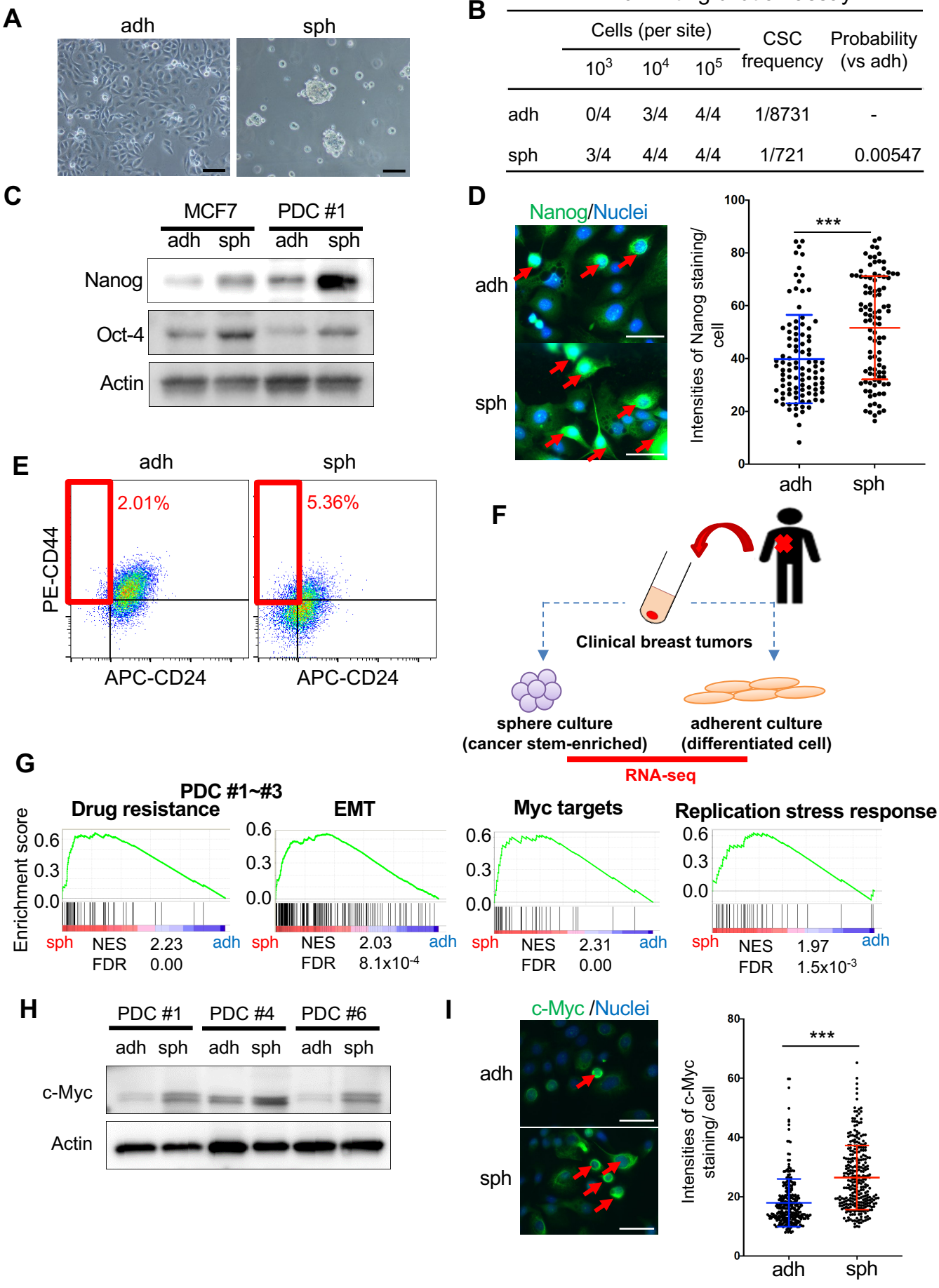
A
adh
sph
B
In vivo limiting dilution assay
Cells (per site)
10^3
10^4
10^5
CSC frequency
Probability (vs adh)
adh 0/4 3/4 4/4 1/8731 -
sph 3/4 4/4 4/4 1/721 0.00547
C
MCF7
PDC #1
adh sph adh sph
Nanog
Oct-4
Actin
D
Nanog/Nuclei
adh
sph
Intensities of Nanog staining/ cell
***
E
adh
sph
2.01%
5.36%
PE-CD44
APC-CD24
APC-CD24
F
Clinical breast tumors
sphere culture (cancer stem-enriched)
adherent culture (differentiated cell)
RNA-seq
G
PDC #1~#3
Drug resistance
EMT
Myc targets
Replication stress response
Enrichment score
sph NES 2.23 adh
FDR 0.00
sph NES 2.03 adh
FDR 8.1x10-4
sph NES 2.31 adh
FDR 0.00
sph NES 1.97 adh
FDR 1.5x10-3
H
PDC #1
PDC #4
PDC #6
adh sph adh sph adh sph
c-Myc
Actin
I
c-Myc /Nuclei
adh
sph
Intensities of c-Myc staining/ cell
***

Figure 2

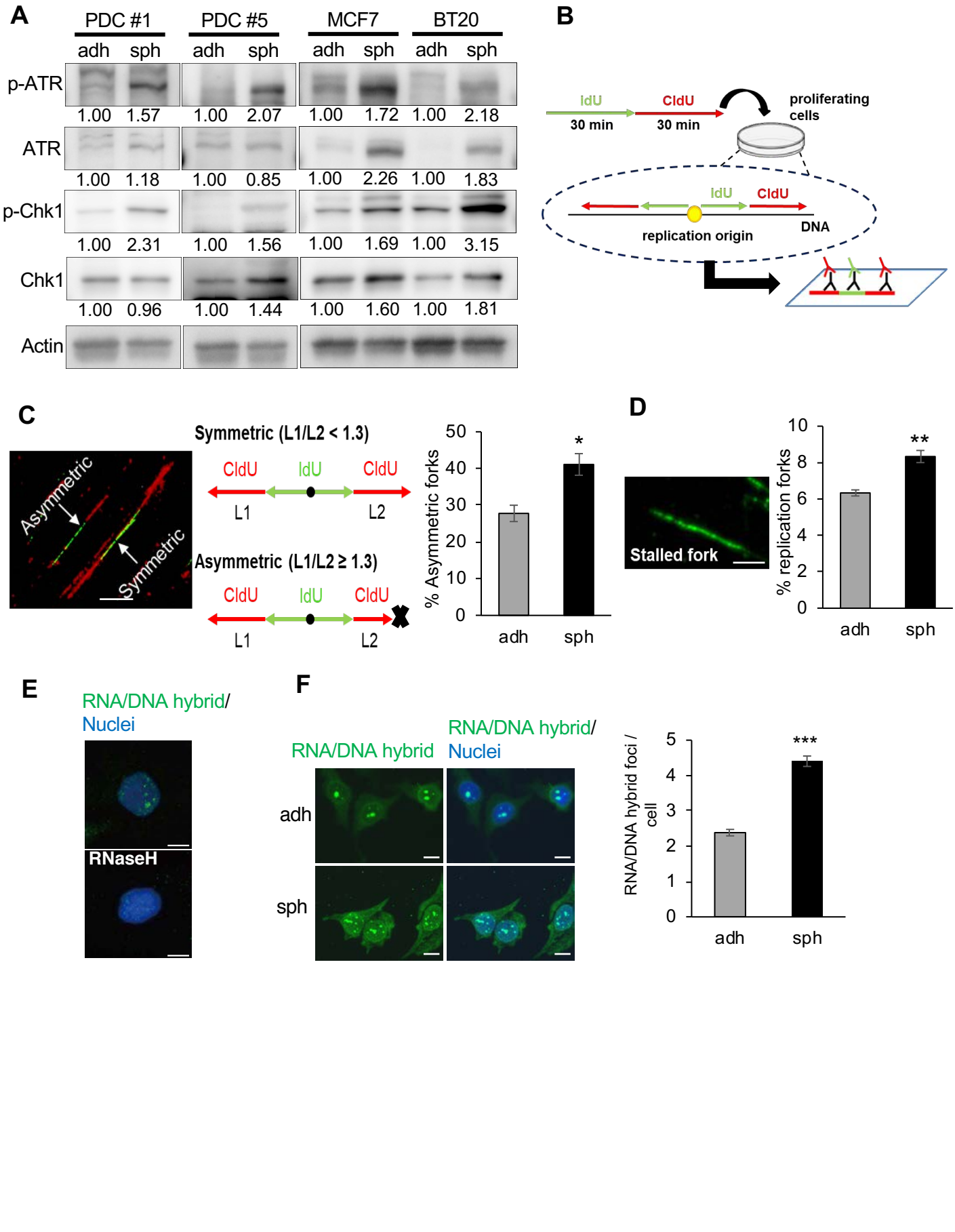
A
PDC #1
PDC #5
MCF7
BT20
adh
sph
p-ATR
1.00 1.57 1.00 2.07 1.00 1.72 1.00 2.18
ATR
1.00 1.18 1.00 0.85 1.00 2.26 1.00 1.83
p-Chk1
1.00 2.31 1.00 1.56 1.00 1.69 1.00 3.15
Chk1
1.00 0.96 1.00 1.44 1.00 1.60 1.00 1.81
Actin
B
IdU
CldU
30 min
30 min
proliferating cells
IdU
CldU
replication origin
DNA
C
Asymmetric
Symmetric
Symmetric (L1/L2 < 1.3)
CldU
IdU
CldU
L1
L2
Asymmetric (L1/L2 ≥ 1.3)
CldU
IdU
CldU
L1
L2
% Asymmetric forks
50
40
30
20
10
0
*
adh
sph
D
Stalled fork
% replication forks
10
8
6
4
2
0
**
adh
sph
E
RNA/DNA hybrid/
Nuclei
RNaseH
F
RNA/DNA hybrid
RNA/DNA hybrid/
Nuclei
adh
sph
RNA/DNA hybrid foci / cell
5
4
3
2
1
0
***
adh
sph

Figure 3

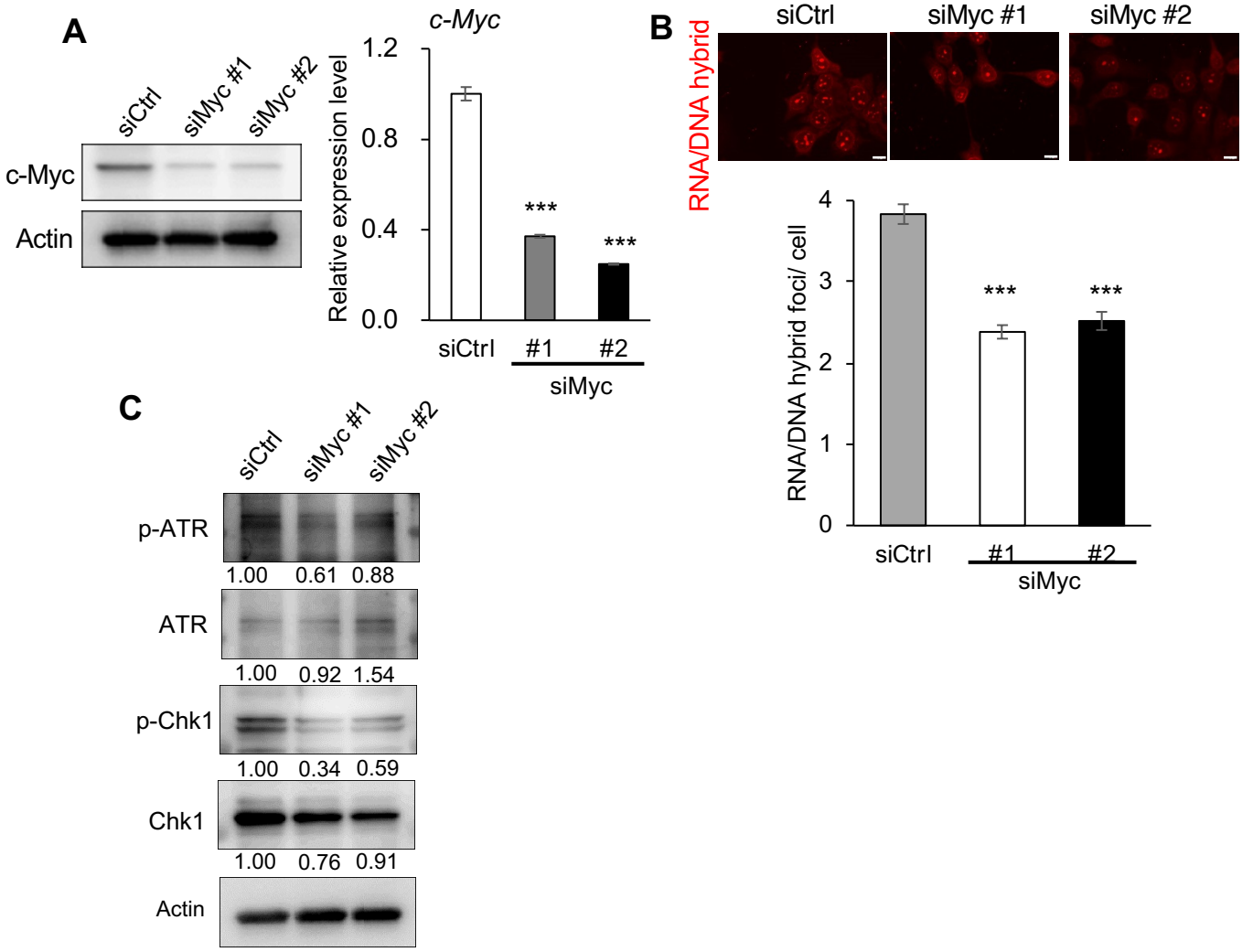
A
siCtrl
siMyc #1
siMyc #2
c-Myc
Actin
c-Myc
Relative expression level
1.2
0.8
0.4
0.0
***
***
siCtrl
#1
#2
siMyc
B
siCtrl
siMyc #1
siMyc #2
RNA/DNA hybrid
RNA/DNA hybrid foci/ cell
4
3
2
1
0
***
***
siCtrl
#1
#2
siMyc
C
siCtrl
siMyc #1
siMyc #2
p-ATR
1.00 0.61 0.88
ATR
1.00 0.92 1.54
p-Chk1
1.00 0.34 0.59
Chk1
1.00 0.76 0.91
Actin

Figure 4

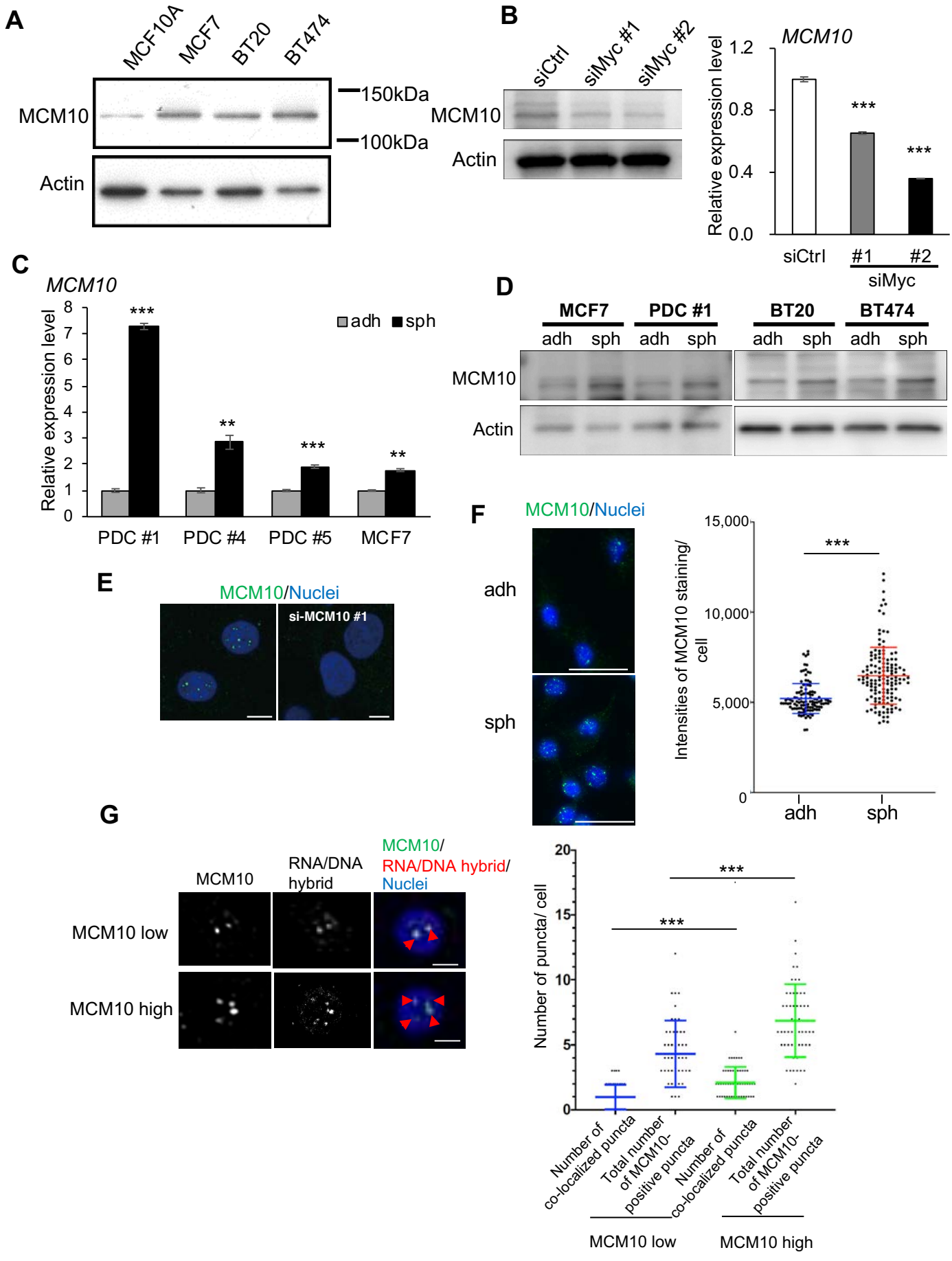
A
MCF10A
MCF7
BT20
BT474
MCM10
Actin
150kDa
100kDa
B
siCtrl
siMyc #1
siMyc #2
MCM10
Actin
MCM10
Relative expression level
1.2
0.8
0.4
0.0
***
***
siCtrl
#1
#2
siMyc
C
MCM10
Relative expression level
adh
sph
***
**
***
**
PDC #1
PDC #4
PDC #5
MCF7
D
MCF7
PDC #1
BT20
BT474
adh
sph
MCM10
Actin
E
MCM10/Nuclei
si-MCM10 #1
F
MCM10/Nuclei
adh
sph
Intensities of MCM10 staining/ cell
15,000
10,000
5,000
0
***
adh
sph
G
MCM10
RNA/DNA hybrid
MCM10/ RNA/DNA hybrid/ Nuclei
MCM10 low
MCM10 high
Number of puncta/ cell
20
15
10
5
0
***
***
Number of co-localized puncta
Total number of MCM10-positive puncta
Number of co-localized puncta
Total number of MCM10-positive puncta
MCM10 low
MCM10 high

Figure 5

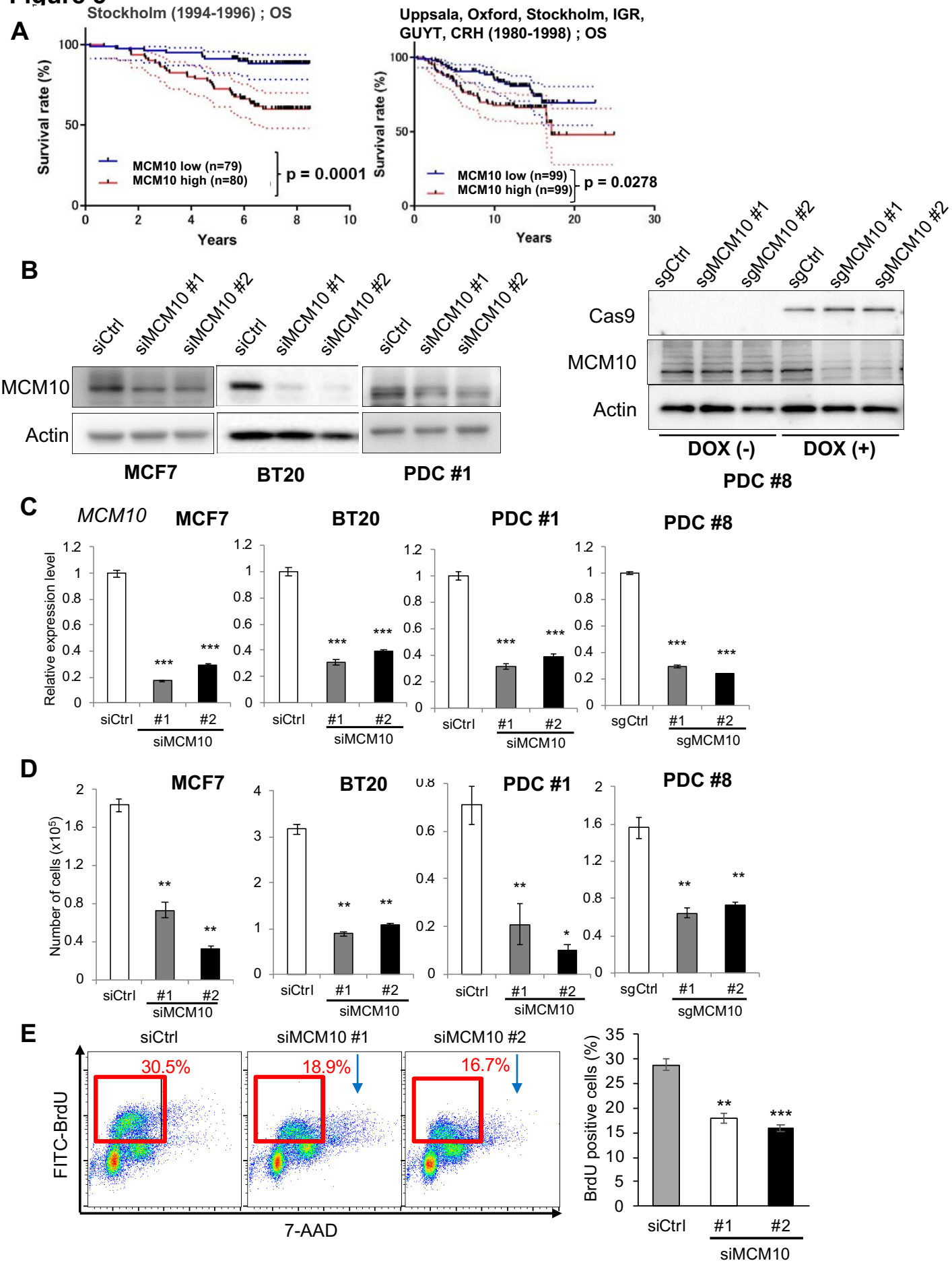
A
Stockholm (1994-1996) ; OS
Survival rate (%)
MCM10 low (n=79)
MCM10 high (n=80)
p = 0.0001
Years
Uppsala, Oxford, Stockholm, IGR, GUYT, CRH (1980-1998) ; OS
MCM10 low (n=99)
MCM10 high (n=99)
p = 0.0278
B
siCtrl
siMCM10 #1
siMCM10 #2
MCM10
Actin
MCF7
BT20
PDC #1
sgCtrl
sgMCM10 #1
sgMCM10 #2
Cas9
DOX (-)
DOX (+)
PDC #8
C
MCM10
Relative expression level
D
Number of cells (x10^5)
E
30.5%
18.9%
16.7%
FITC-BrdU
7-AAD
BrdU positive cells (%)

Figure 6

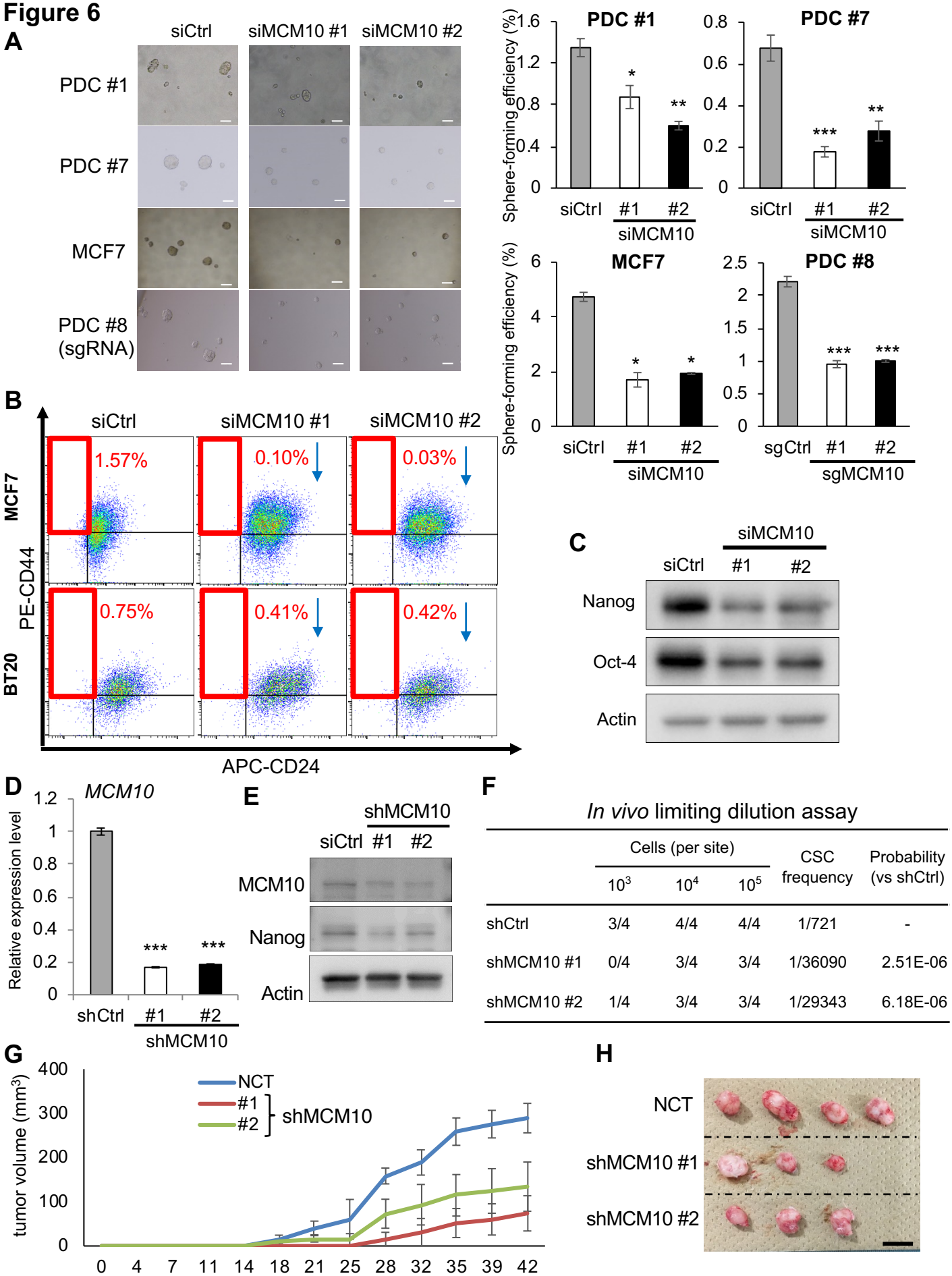

	Cells (per site)			CSC frequency	Probability (vs shCtrl)
	10^3	10^4	10^5		
shCtrl	3/4	4/4	4/4	1/721	-
shMCM10 #1	0/4	3/4	3/4	1/36090	2.51E-06
shMCM10 #2	1/4	3/4	3/4	1/29343	6.18E-06

Figure 7

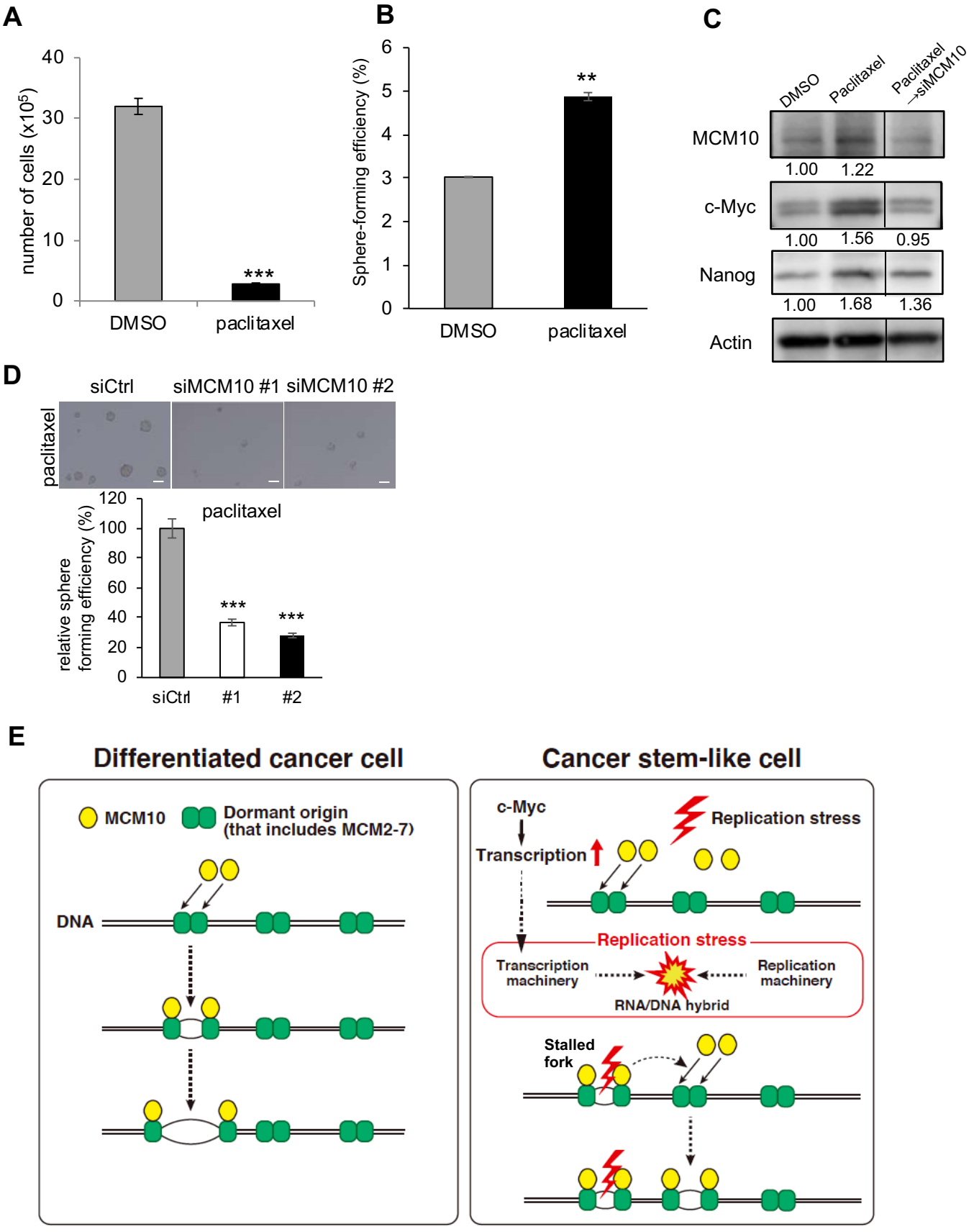
A
number of cells (x10^5)
40
30
20
10
0
***
DMSO
paclitaxel
B
Sphere-forming efficiency (%)
6
5
4
3
2
1
0
**
DMSO
paclitaxel
C
DMSO
Paclitaxel
Paclitaxel →siMCM10
MCM10
1.00
1.22
c-Myc
1.00
1.56
0.95
Nanog
1.00
1.68
1.36
Actin
D
siCtrl
siMCM10 #1
siMCM10 #2
paclitaxel
paclitaxel
relative sphere forming efficiency (%)
120
100
80
60
40
20
0
***
***
siCtrl
#1
#2
E
Differentiated cancer cell
MCM10
Dormant origin (that includes MCM2-7)
DNA
Cancer stem-like cell
c-Myc
Transcription
Replication stress
Replication stress
Transcription machinery
Replication machinery
RNA/DNA hybrid
Stalled fork

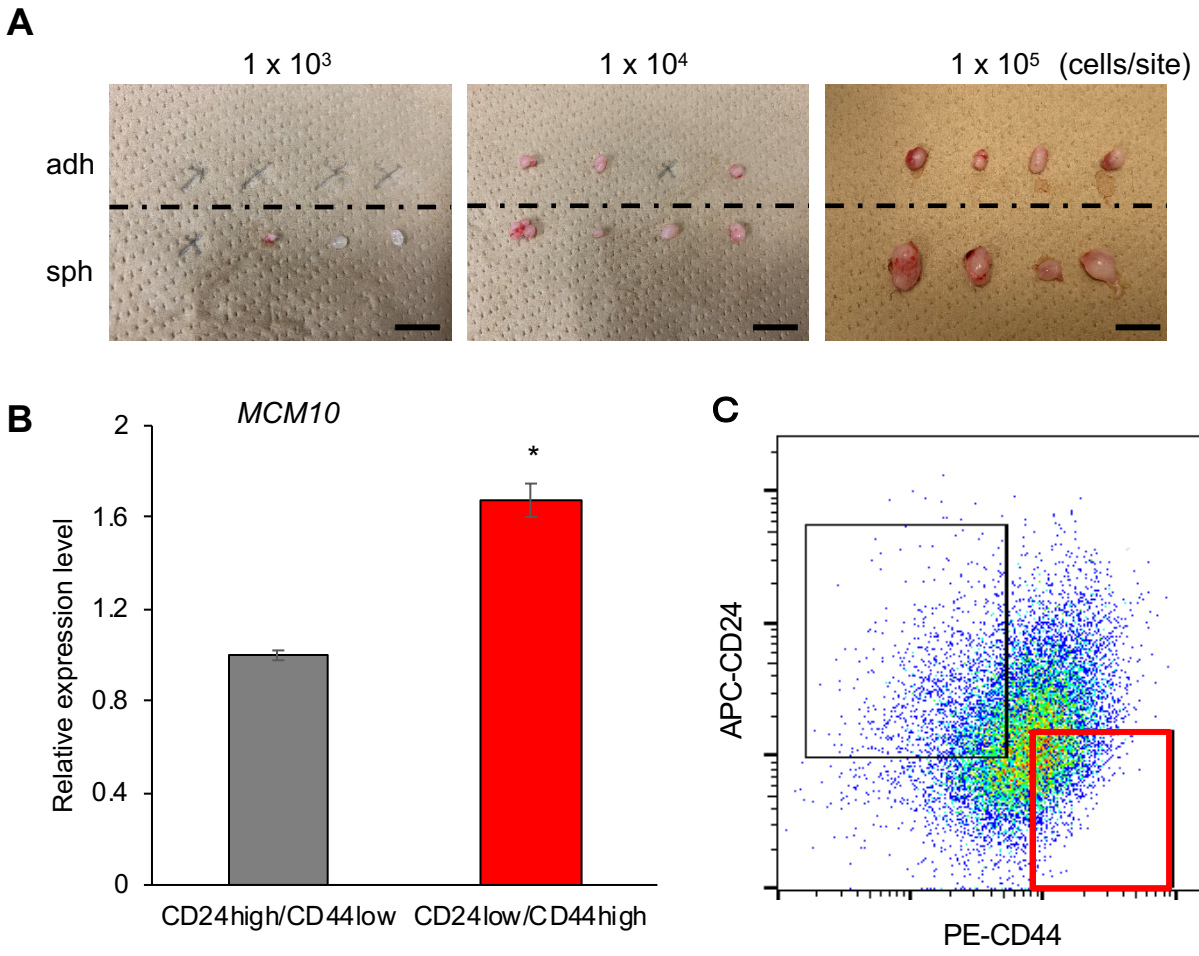

Supplementary Figure 1. a, Representative images of tumors formed in the *in vivo* limiting dilution assay (1×10^3, 10^4 and 10^5 cells/site). Scale bar = 10 mm. **b** ,**c**, Expression level of *MCM10* was compared by qPCR between the $CD24^{-/low}/CD44^{high}$ CSC-enriched population and the $CD24^{high}/CD44^{low}$ control population. The PDC #6 cells were analyzed. (mean ± SEM, n = 3; *p < 0.05).

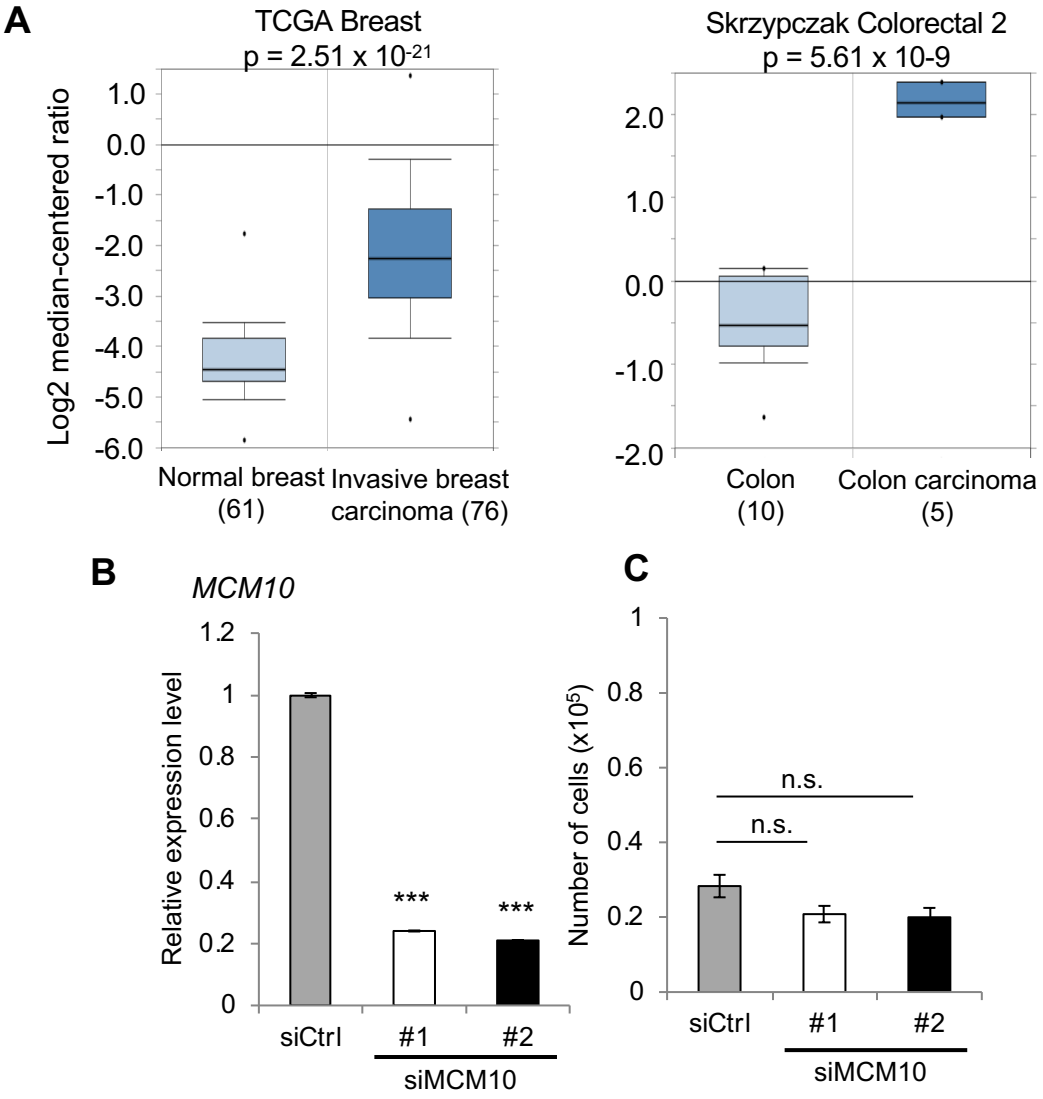

Supplementary Figure 2. a, *MCM10* expression was compared between non-malignant cells and cancer cells in breast and colon using the Oncomine cancer gene expression database (Right; TCGA Breast, Left; Skrzypczak Colorectal 2). P-values were calculated by Student's t-test. **b,c**, MCF10A treated with siCtrl or *siMCM10*. Knockdown efficiencies of siRNAs (**b**) and growth rates (**c**) were compared.

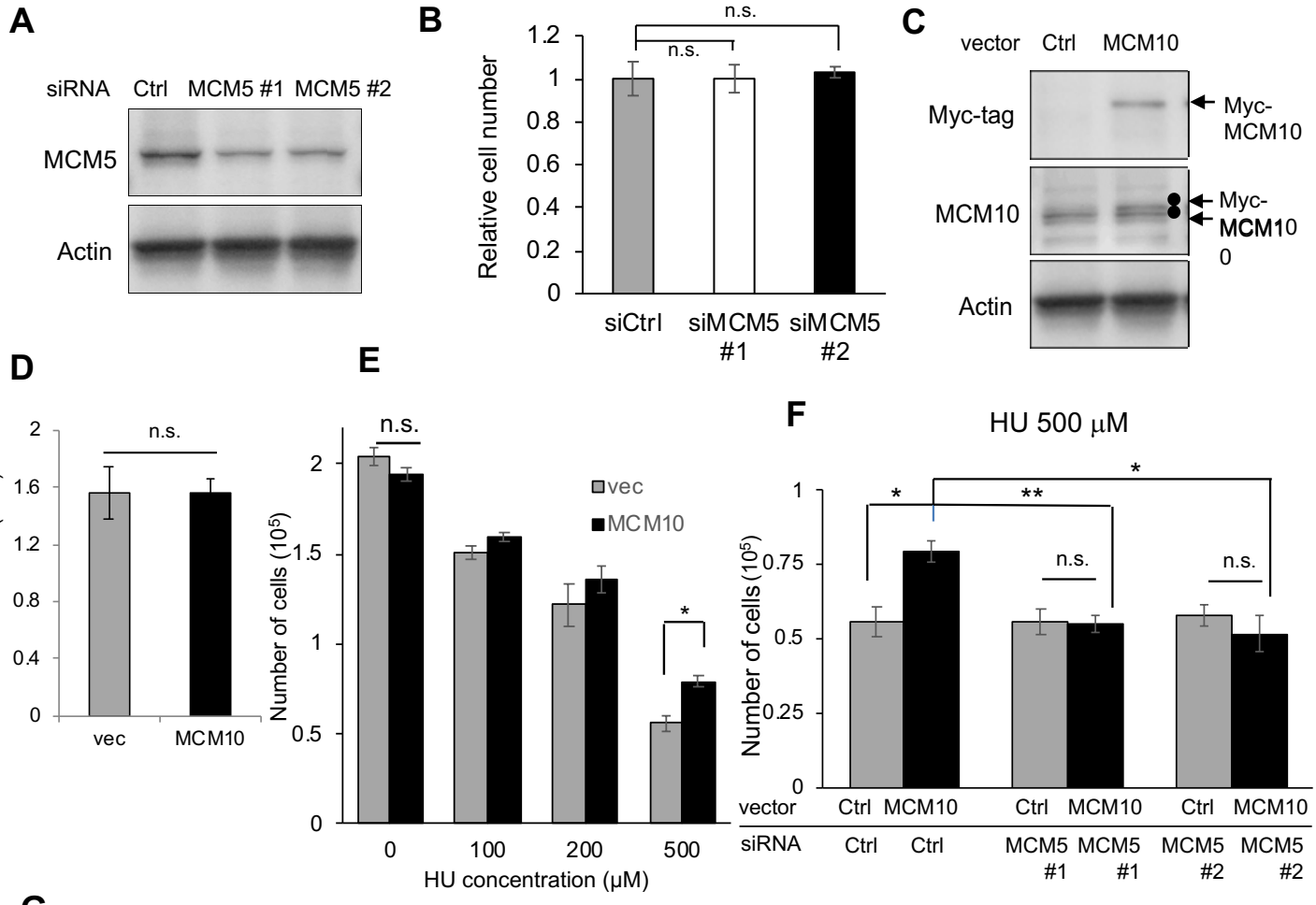

G

In vitro limiting dilution assay

	Cells (per site)						CSC frequency	Probability (vs shCtrl)
	63	125	250	500	1000	2000		
shCtrl	0/8	1/8	5/8	7/8	8/8	8/8	1/319	-
shMCM10 #1	0/8	0/8	1/8	4/8	8/8	8/8	1/652	0.0456
shMCM10 #2	0/8	0/8	1/8	3/8	8/8	8/8	1/716	0.0241

Supplementary Figure 3. a, b, Expression levels of MCM5 were compared in MCF7 cells treated with siCtrl or *siMCM5* (**a**). Number of cells were counted after 4 days (mean ± SEM, n = 3) (**b**). **c,d**, Expression levels of endogenous MCM10 and Myc-tagged MCM10, as determined by immunoblotting, were compared among cells transfected with the indicated expression vectors (**c**). Number of cells were counted after 4 days (mean ± SEM, n = 3)(**d**). **e,f,** MCF7 cells transfected with the indicated vectors (**e**) and siRNAs (**f**) were seeded in a 12-well plate (10,000 cells/well). Forty-eight hours later, they were treated with indicated concentrations of HU for an additional 48 h. Cells were harvested and counted (mean ± SEM, n = 3; $^{**}p < 0.01$, $^{*}p < 0.05$). **g**, In vitro limiting dilution assay for MCM10-depleted cells in patient-derived breast cancer cells: 2,000, 1,000, 500, 250, 125, or 63 cells were seeded in each well of a 96-well ultra–low-attachment plates. Results were obtained 7 days after seeding. CSC frequency and p-values were determined using the ELDA software.

Supplementary Table 1. Characteristics of clinical breast tumors used in this study

PDC #	ER	PgR	HER2	Molecular subtypes
1	-	-	0	Triple negative
2	3+	3+	2+ (FISH+)	Luminal HER2
3	3+	-	3+	Luminal HER2
4	-	-	2+ (FISH+)	HER2
5	-	-	2+ (FISH-)	Luminal like
6	+	+	2+ (FISH-)	Luminal like
7	-	+	-	Luminal like
8	-	-	-	Ovarian cancer

Supplementary Table 2. Genes included in Reactome_DNA_Replication gene set and the ratios of expression levels of each gene, sphere cells (SPH) / adherent cells (ADH)

Rank	Gene symbol	SPH/ADH
1	GMNN	37.044
2	SPC25	28.289
3	RPS27A	27.516
4	PSME1	21.896
5	MCM10	15.916
6	CDT1	15.123
7	PSMC2	13.974
8	CENPI	13.831
9	AURKB	12.728
10	CDC6	12.029
11	BIRC5	9.943
12	GINS2	9.823
13	SKA1	9.493
14	NDC80	9.282
15	CENPM	8.938
16	ERCC6L	8.639
17	PSMD9	8.307
18	NUF2	7.717
19	CDC45	7.440
20	KIF2C	7.041
21	NUDC	7.037
22	PRIM1	6.714
23	ZWINT	6.504
24	CDCA8	6.473
25	CENPK	6.246
26	MLF1IP	5.954
27	ZWILCH	5.924
28	KIF18A	5.346
29	GINS1	5.281
30	FEN1	5.251
31	E2F1	4.845
32	GORASP1	4.819
33	CENPA	4.714
34	PLK1	4.472
35	SGOL2	4.429
36	BUB1	4.375
37	E2F2	4.169
38	ITGB3BP	4.135
39	TAOK1	3.893
40	PCNA	3.872
41	ORC6	3.823
42	SMC3	3.778
43	MCM5	3.717
44	CENPQ	3.709
45	SGOL1	3.628
46	RFC3	3.606
47	CDC7	3.542
48	KIF23	3.485
49	APITD1	3.353
50	BUB1B	3.351
51	CENPL	3.325
52	ORC1	3.265
53	RFC2	3.244
54	PPP2R5B	3.204
55	CDC20	3.180
56	MCM4	3.153
57	RANBP2	3.138
58	MCM6	3.083
59	CENPN	3.048
60	PPP2R5A	2.991
61	INCENP	2.967
62	MCM7	2.926
63	POLD3	2.837
64	CASC5	2.796
65	PSMA1	2.785
66	KIF20A	2.776
67	RAD21	2.735
68	DNA2	2.724
69	LIG1	2.710
70	CENPP	2.706
71	SKA2	2.696
72	SPC24	2.657
73	PPP2CB	2.635
74	MAD2L1	2.634
75	FBXO5	2.612
76	CDKN1A	2.611
77	RPA3	2.554
78	CCNA1	2.552
79	CENPO	2.513
80	DSN1	2.460
81	MCM3	2.456
82	NUP85	2.418
83	PSMF1	2.379
84	DBF4	2.332
85	MCM8	2.249
86	POLE	2.223
87	PSMC4	2.145
88	SEC13	2.123
89	MCM2	2.109
90	STAG1	1.914
91	PSMA8	1.895
92	PPP2R1A	1.836
93	NUP133	1.833
94	SMC1A	1.804
95	PSMC5	1.799
96	PPP2R5E	1.790
97	ORC2	1.776
98	PSMD10	1.773
99	NUP37	1.771
100	BUB3	1.767
101	NSL1	1.746
102	PSMC3	1.743
103	PSMA3	1.739
104	PMF1	1.733
105	RPA2	1.720
106	PSMA5	1.707
107	PSMD11	1.700
108	RPA1	1.698
109	CENPT	1.646
110	PSMB7	1.645
111	PSMD12	1.644
112	PSMD1	1.634
113	PSMA2	1.616
114	PAFAH1B1	1.608
115	PSMD6	1.595
116	POLD2	1.564
117	PSMA7	1.533
118	RFC4	1.528
119	POLA2	1.519
120	CLIP1	1.509
121	PSME2	1.509
122	POLE2	1.489
123	PSMB1	1.467
124	UBA52	1.466
125	CCNA2	1.461
126	PSMB5	1.451
127	ORC4	1.405
128	PSMD14	1.402
129	PSMD8	1.377
130	ORC3	1.366
131	PSMB8	1.352
132	PSMD13	1.344
133	PSMD2	1.336
134	MIS12	1.320
135	XPO1	1.316
136	PSMD4	1.282
137	GINS4	1.275
138	NUP107	1.271
139	CENPH	1.269
140	PSMA6	1.253
141	ORC5	1.211
142	ZW10	1.187
143	PRIM2	1.182
144	PSMB9	1.167
145	PSMB6	1.157
146	NUP43	1.156
147	POLA1	1.147
148	PSMD7	1.138
149	RB1	1.131
150	AHCTF1	1.129
151	PSMA4	1.128
152	PSMB3	1.114
153	CDKN1B	1.108
154	PPP2R5C	1.108
155	PPP2CA	1.105
156	PPP2R1B	1.103
157	CDK2	1.094
158	PPP1CC	1.020
159	MAD1L1	0.989
160	PPP2R5D	0.896
161	PSMD3	0.885
162	PSMB4	0.880
163	MAPRE1	0.868
164	PSMB10	0.844
165	KIF2A	0.822
166	KNTC1	0.814
167	E2F3	0.773
168	PSMD5	0.768
169	STAG2	0.766
170	POLD4	0.695
171	SEH1L	0.626
172	PSMB2	0.624
173	PSMC6	0.610
174	RFC5	0.548
175	PSME4	0.533
176	RCC2	0.502
177	CKAP5	0.496
178	NDEL1	0.472
179	CLASP1	0.438
180	RANGAP1	0.436
181	CENPC1	0.417
182	B9D2	0.320
183	PSMC1	0.121
184	RPS27	0.020